Spatial variation in cost of electricity-driven continuous ammonia production in the United States

Abhishek Bose,[†] Nikifar Lazouski,[‡] Michal Gala,[‡] Karthish Manthiram,[‡] and Dharik S. Mallapragada[*,†]

†*MIT Energy Initiative, Massachusetts Institute of Technology, Cambridge, USA*

‡*Department of Chemical Engineering, Massachusetts Institute of Technology, Cambridge, USA*

E-mail: dharik@mit.edu

Abstract

Cost-effective, low-carbon ammonia production is necessary for decarbonizing its existing uses, but could also enable decarbonization of other difficult-to-electrify end-uses like shipping where energy density is a key criterion. Here, we assess the levelized cost of ammonia production (95% availability) at industrial-scale quantities (250 tonnes/day) in 2030 from integrating commercial technologies for renewable electricity generation, electrolysis, ammonia synthesis and energy storage. Our analysis accounts for the spatial and temporal variability in cost and emissions attributes of electricity supply from variable renewable energy (VRE) sources and the grid, and its implications on plant design, operations, cost and emissions. Based on 2030 technology cost and grid projections, we find that grid-connected ammonia in the midcontinental U.S. costs 0.54-0.64 $/kg, as compared to 0.3-0.4 $/kg for natural gas-based ammonia and depending on the generation mix of the grid, may have higher or lower CO_2 emissions.

Fully VRE-based ammonia production, even with simultaneous wind and PV utilization, is more expensive than grid connected outcomes, due to the need for storage to manage VRE intermittency and continuous ammonia production. Instead, using VRE and grid electricity for ammonia production under moderate carbon policy (50$/tonne CO_2 price) in the midcontinental U.S. can achieve 55-100% CO_2 emissions reduction per tonne of ammonia compared to natural gas routes and corresponds to levelized cost range of 0.54-0.63 $/kg NH_3). Further cost reductions are shown to be possible if the ammonia synthesis loop can be made more flexible, which reduces the need for round-the-clock electricity supply and the substitute use of battery storage with ammonia storage.

Introduction

Global efforts for reducing greenhouse gas (GHG) emissions over the past decade have seen the most success in the electric power sector, while emissions from other sectors have seen only modest declines or remained stagnant. For example, in the U.S., CO_2 emissions from the power sector declined by 26% during 2008-2018, while for the same period, transportation CO_2 emissions increased by 1.4% and industrial CO_2 emissions decreased by 9%.[1] Decarbonization strategies for these sectors often cite electrification as a potential pathway, which shifts the burden of emissions reduction from these sectors to the power sector, where continued growth of wind and solar generation is expected to further reduce the emissions intensity of the electricity supply. While direct electrification of certain end uses is poised to grow rapidly (e.g. light-duty vehicles), it may be challenging in particular applications such as heavy-duty transport like shipping and aviation where high energy density requirements remain a key performance criterion. For these end uses, using alternative energy carriers like hydrogen (H_2) and by extension hydrogen-rich molecules like ammonia (NH_3) and other liquid fuels, produced using low-carbon pathways, remain an appealing prospect.

Ammonia offers some distinct advantages over other energy carriers, such as being carbon-

free at point of use, increased volumetric energy density vs. compressed H_2, ease of storage and transport compared to liquid or gaseous H_2 and long-track record for safe handling at scale.[2–4] The predominant route for ammonia production today relies on fossil fuels such as natural gas and coal as a source of energy and hydrogen for thermochemical Haber-Bosch (H-B) synthesis, and is estimated to result in about 2.3 tonnes of CO_2 per tonne NH_3 produced.[5] The reliance on natural gas for ammonia production also implies that cost of natural gas is a key driver of the effective landed cost of the ammonia, ranging from 300-400 $/tonne in the U.S. context[6] to higher prices near 700 $/tonne for other regions with limited domestic natural gas supply and infrastructure constraints, such as India and Africa.[7–9]

Declining costs of variable renewable energy (VRE)-based electricity and electrolyzers have raised interest in producing low-carbon H_2 via electrolysis, as well as its use in decarbonization of industrial ammonia production.[10–13] This route is among the most technologically mature process concepts for electricity-based ammonia production[14–16] and paves the way for emerging electrochemical ammonia production pathways that are modular and hence, amenable to deployment at smaller scales as compared to the conventional fossil-fuel-driven process.[14,17] As noted earlier, electrically-driven ammonia production is potentially appealing for many developing countries with relatively high natural gas costs, and where ammonia use for fertilizer is projected to grow rapidly over the next few decades.[17] Finally, the ease of handling and storage of liquid ammonia relative to hydrogen also opens up the potential for use of ammonia as a potential energy storage vector in a carbon-constrained world.[5,18]

Several recent studies have investigated the techno-economics of electrically driven ammonia production process via low temperature electrolytic hydrogen production coupled with thermochemical H-B synthesis. These studies tend to focus on one or more the following aspects: a) NH_3 costs in a particular geographical region, including the Middle East,[19] Iceland,[20] Germany,[21] Chile,[22] China[23] and India,[24] b) alternate electricity supply options, ranging from co-located VRE supply as part of islanded systems,[25] to grid+contractual VRE

supply via power purchase agreements,[26] c) representation of ammonia production requirements and process operational constraints, which are included in varying detail by some studies[21,27,28] but overlooked in other cases[25,29–31] and d) inclusion of alternative on-site storage technologies to manage temporal variability in electricity supply, either from the grid or on-site or contracted VRE sources.[22,26,28,32] Here, we note the salient contributions of some of these studies, while noting their differentiating aspects related to model fidelity (i.e. temporal resolution, demand and operational constraints), regional characteristics and level of decarbonization evaluated (see Table 1). Nayak-Luke et al.[25] evaluate the effect of VRE electricity on running a thermochemical Haber-Bosch process reactor with electrolytic H_2 supply. They model electricity supply from different combinations of co-located PV and wind generation while optimizing for the H-B system size that also accounts for process flexibility. However, the authors do not model grid-based electricity supply or the full-spectrum of storage options to manage VRE variability. Banares-Alcantara et al.[33] evaluate the levelized cost for an islanded ammonia generation facility, but overlook temporal variations in VRE generation. Morgan et al.[30] study offshore wind driven ammonia production in the United States (U.S.) context while incorporating intermediate storage for the physical ammonia process components but overlook the time and price variations in grid and wind farm power output and its impact on hourly process operations and overall cost. Osman et al.[28] develop a techno-economic model that incorporate the effects of variability in solar resources, the flexibility of the subsystems such as air separation unit (ASU), electrolyzers as well as an ASPEN based process model, to study design and operations of a renewable ammonia system in the Middle East. However they overlook the role of grid integration which, as we discuss in later sections, may allow for lowering ammonia costs and eventually CO_2 emissions as well. On similar lines, Armijo et al.[34] focus on studying the potential for renewable ammonia production in Chile & Argentina through a temporally resolved optimization model and conclude that the combination of wind and solar resources for electricity supply can drive down costs by reducing the overall variability in energy supply. The authors

also study the role of flexible H-B process operation as a key driver for eventual reduction of costs. Schulte Beerbuhl et al[35] develop a design and operations model for electricity-based ammonia production that includes non-linear constraints related to some unit operation (e.g. electrolyzer) which is shown to provide a more accurate representation of process flexibility. Related to this, Allman et al.[36] have focused on evaluating the effects of wind intermittency on cost of ammonia production in the US upper Midwest. The authors also study the role of intermediate N_2 and H_2 storage to ensure round-the-clock operation. Palys and Daoutidis also consider storage of intermediate H_2 and N_2 along with NH_3 as part of designing a renewable energy storage and supply system for meeting MW-scale electricity demand.[32] Due to the many unit operations choices being considered, the resulting design optimization model considers plant operation over a limited number (672) of representative periods while preserving chronology that is important to model seasonal energy storage.[32]

Table 1: Summary of recent work on electricity driven ammonia production techno-economic modeling

Reference	VRE Sources Considered	Modelled Operations Variability?	Grid Connection?	H-B Synthesis Loop Process Model?	Storage Options	H-B Process Flexibility?	Region
Nayak Luke et al.[25]	PV, Wind	Yes	No	No	H_2 only	Yes	UK
Guerra et al.[22]	No	No	PPA	No	NH_3 only	No	Chile
Maia et al.[20]	Wind	No	No	No	NH_3 only	No	Iceland
Osman et al.[28]	PV, CSP	Yes	No	Yes	H_2, N_2, NH_3	No	UAE
Morgan et al.[30]	Wind	No	Yes	No	H_2, N_2, NH_3	No	USA
Beerbuhl et al.[35]	No	Yes	Yes	No	H_2 only	No	Germany
Allman et al.[36]	Wind	Yes	No	No	H_2, N_2, NH_3	No	USA
Nosherwani et al.[21]	Wind	Yes	No	Yes	H_2, N_2, NH_3	No	Brazil
Liang et al.[27]	-	-	-	Yes	-	Yes	Netherlands
Zhang et al.[37]	-	-	Yes	Yes	-	No	Italy
Palys and Daoutidis[32]	PV, Wind	Yes	No	No	H_2, N_2, NH_3	Yes	USA
Current Work	PV, Wind	Yes	Yes	Yes	H_2, N_2, NH_3, Li-ion	Yes	USA

In this study, we perform a detailed spatial and temporally resolved analysis of electrically driven ammonia production via the process depicted in Figure 1. Our analysis is based on modeling the least cost design and operation of the process while considering three key attributes influencing the overall process economics: a) temporal variability in electricity supply from grid and co-located VRE generation, b) detailed process considerations, including operational inflexibility of the thermochemical H-B synthesis as well economies of scale of investment in certain unit operations, and c) use of alternate on-site storage options to manage temporal variability in energy inputs, including chemical storage and electricity storage. We use the developed model to evaluate cost of electricity-based NH_3 supply for various regions in the continental U.S. under various technology cost assumptions, carbon policy and electricity supply scenarios (dedicated VRE or grid based, VRE + grid) for 2030. Finally, we use the model to explore the economic value and process design implications of introducing limited operational flexibility in thermochemical H-B synthesis.

Methodology

The integrated design and operations modeling framework used in this study is adapted from prior work[38] and incorporates the unique features influencing design and operations of industrial processes like ammonia production: a) round-the-clock operation to maximize capacity utilization, b) centralized production to maximize economies of scale of thermochemical processes and c) limited operational flexibility owing to large thermal inertia of units, and d) extensive heat and mass integration within the process. We formulate the design and operations assessment as a mixed integer linear program (MILP) with an objective function corresponding to the sum of the annualized investment (CAPEX) and operating (OPEX) cost of running the ammonia production facility shown in Figure 1. This objective is minimized subject to a variety of operational and policy constraints that are enforced to model plant operations throughout the year at a hourly resolution, resulting in 8760 opera-

tional periods. The resulting MILP model is solved via Gurobi[39] run on a Xeon-g6 processor with 4 GB of RAM across 32 cores on each compute node.[40] The average time to converge for each run ranges from 200-900 seconds considering an optimality gap of 5% or lower. The base system design parameters are shown in Table 2. Below, we describe the modeling of the various unit operations in the process along with a summary of the key cost and performance assumptions impacting their design and operations, with additional details provided in the supporting information (SI).

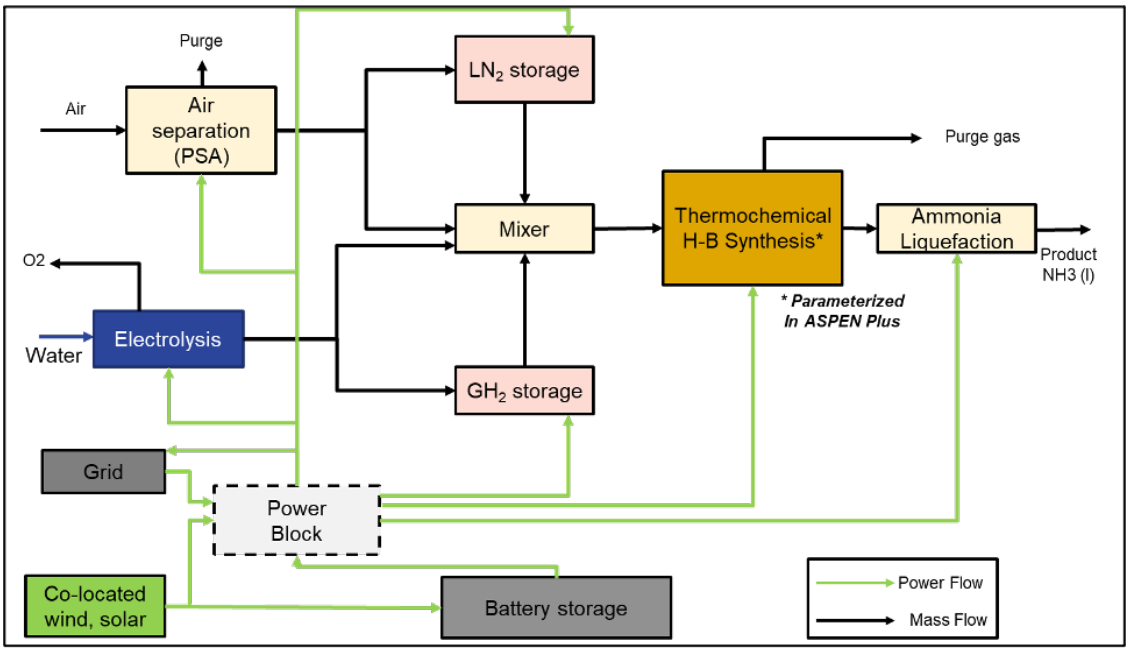

Figure 1: Simplified process flow diagram of ammonia production process based on electrolytic H_2 supply and thermochemical Haber-Bosch (H-B) Synthesis. Detailed ASPEN model used to evaluate H-B synthesis is provided in appendix (see Figure SI 10) in supporting information (SI). PSA = Pressure Swing Adsorption. H-B = Haber-Bosch. LN2 = Liquid Nitrogen. GH2 = Gaseous hydrogen.

Electrolyzer

H_2 production via low-temperature electrolysis is modeled based on available cost and performance projections for proton exchange membrane (PEM) electrolyzers for 2030[41] (see

Table 2: Design assumptions for electricity-driven ammonia process

Parameter	Value	Units
Ammonia production capacity	250	$tonnes/day$
Plant minimum down time	48	$hours$
CAPEX contingency factor	21	%
Discount rate	8	%
Weather year for renewable availability data	2011	
Cooling water use	1000	$tonnes/tonne NH_3$
Cooling water cost	0.0148	$\$/tonne$
Plant annual availability	95%	
Grid interconnection cost	30	$\$/kW$

Supplementary Table SI 1 for assumptions). PEM electrolyzer capital costs projections reported in the literature vary greatly, reflecting the emerging nature of this technology as well as scales at which capital costs are quoted (e.g. kW vs. 1 or 10's of MW[42]). Here we model PEM capital costs of 500 \$/kW (see Table SI 1), based on projections for multi-MW scale systems[41–43] that would needed for the modeled ammonia production facility (250 tonne/day). We assume electrolyzer lifetime of 20 years, with the cost of periodical stack replacement included as part of the FOM cost (5%, see Table SI 1). PEM electrolyzers can produce pressurized H_2 at 30 bar which could be stored as a compressed gas for later use as feed for H-B synthesis. The model sizes the optimal electrolyzer capacity as well as enforces hourly operational constraints to track the power inflow into the system and produced H_2 stream flow rates to the storage and H-B unit (Eqn:19,18 in SI). We also enforce the requirement that PEM electrolyzer production must either be constrained above a minimum loading level, set at 5% of nameplate capacity, or switched off.[42] This behavior is modeled using a binary variable in each time period that tracks whether the electrolyzer is on or off (Eqn: 22. The cost impact of including this operating constraint is negligible (0.3%, see Fig. SI 9), presumably because the minimum power load is quite low. However, the model with the additional variables and constraints to model the minimum power load takes about four times longer to solve as compared to the model without these variables or constraints, implying that ignoring them could have a small cost impact but relatively large run time

impact.

Storage

We model four forms of storage using a common structure that separates sizing decisions related to storage capacity (energy or mass) and maximum rate of charging or discharging storage. The four storage types include: a) Li-ion battery storage, b) Gaseous hydrogen (above-ground storage), c) Liquid nitrogen, and d) ammonia storage as a pressurized gas or liquid. Storage operation is modeled to follow constraints that track storage inventory levels from one hour to the next, as well as adherence to the installed capacity limits (see Eq. 10-12). We consider availability of ammonia storage only in the case when the H-B process is modeled to be flexible. Storage parameters are summarized in Table SI 4.

Air separation unit

Nitrogen (N_2) generation is modeled as per the specifications of the pressure swing adsorption (PSA) process (see Table SI 2), that can adjust its hourly output flexibly. PSA units tend to operate in a cyclical steady-state and this mode of operations allows for operational flexibility that can be leveraged in an electrically-driven ammonia production process.[44] To account for the economies of scale in the PSA process, we model the capital cost of the system as a piece-wise linear function of capacity using 5 piece-wise linear segments (see Eq. 13-15 in SI). The N_2 output from PSA is then split into two streams - directly flowing into the H-B synthesis loop or being liquefied for storage. The stored liquid N_2 is pumped into the H-B stream at the reactor pressure (250 bar) for further use.

Haber-Bosch (H-B) synthesis loop

The H-B synthesis loop section is simulated in ASPEN plus based on the flowsheet shown in Figure 1, starting with input of pure H_2 and N_2 streams from the upstream production

facilities. The H-B synthesis loop consists primarily of three sections: a) the compressor train to compress the input feed gas (mixture of H_2 and N_2) to 250 bar for the H-B reactor, b) the H-B reactor which is maintained at a temperature of 500°C with a heat recovery exchanger to recover waste heat from the output stream (Eq. 24-29) and c) finally a flash tank which separates and liquefies the output NH_3 in the system to produce liquid ammonia (99% purity)(Eq. 35-36). For the MILP model, the H-B synthesis loop is treated as a black box with pre-defined process operating parameters related to power and cooling water inputs from the ASPEN simulation (see Table SI 2).

Currently deployed H-B synthesis facilities tend to operate at steady-state and we have incorporated this constraint in our modeling. At the same time, to understand the role of flexible H-B synthesis and the impact on cost - we introduce three parameters to understand the nature of flexibility in the synthesis loop: minimum stable production level, minimum shutdown times and ramp rates. The minimum shutdown constraint (Eq. 31) enforces that the plant has to be remain shutdown for a minimum amount of time (assumed to be 48 hours based on 10°C/hour rate of temperature increase for the reactor)[45] before being brought back to full production (Eq. 33-34).

Electricity supply

Electricity is the only energy input for the entire process and we consider the availability of VRE resources (solar (PV) and wind) as well as connections to the grid (including grid interconnection + electricity supply costs and emissions) as a part of the set of available electricity sources. The model takes inputs in the form of hourly VRE capacity factor data as well as electricity price time series (see Eqns.:8, 9 in SI).

VRE resource modeling

To characterize VRE availability over the continental U.S., we define a grid consisting of 1487 nodal points across the region. Then for each grid point, the renewable energy resource

availability profile is generated in line with Brown and Botterud[46] and summarized in SI. We consider renewable availability data for 2011 as a representative weather year for our analysis.

Table 3: VRE Resource Cost assumptions. Cost assumptions reflect 2030 projections available from the literature[47]

Resource	CAPEX *$/kW*	FOM *%*	Lifetime *years*	Reference
PV	500	1	20	[47]
Wind	1200	2	20	[47]

Grid Electricity Input

To evaluate the cost and emissions impact of grid electricity supply on electricity-based ammonia production, we evaluated model scenarios using spatially and temporally-resolved electricity system projections for 2030 available from National Renewable Energy Laboratory (NREL)'s 2020 standard scenarios.[48,49] Specifically, we use simulated electricity prices and marginal emission factors data for 2030 for each balancing area corresponding to NREL's mid-range renewable penetration scenario. The spatial distribution in CO_2 emissions intensity and marginal electricity prices for the region under focus in our study is presented in Figure 2 and Figure SI 1, respectively.

While there are no direct CO_2 emissions from the process shown in Figure 1, we account for the CO_2 emissions associated with the grid electricity supply in the model, which allows for holistic assessment of shifting from natural gas to electricity driven processes. Therefore, the hourly electricity requirement from the grid is tracked and the corresponding marginal CO_2 emissions intensity of the supplied grid electricity at each time period is incorporated in computing the CO_2 emissions intensity of ammonia production. Marginal emission factors are modelled in place of average emissions to account for the hourly variability in grid operations.[50] As discussed in the results, this representation of grid electricity use allows for exploring trade-offs between grid supply vs. co-located VRE supply under various CO_2

policy scenarios.

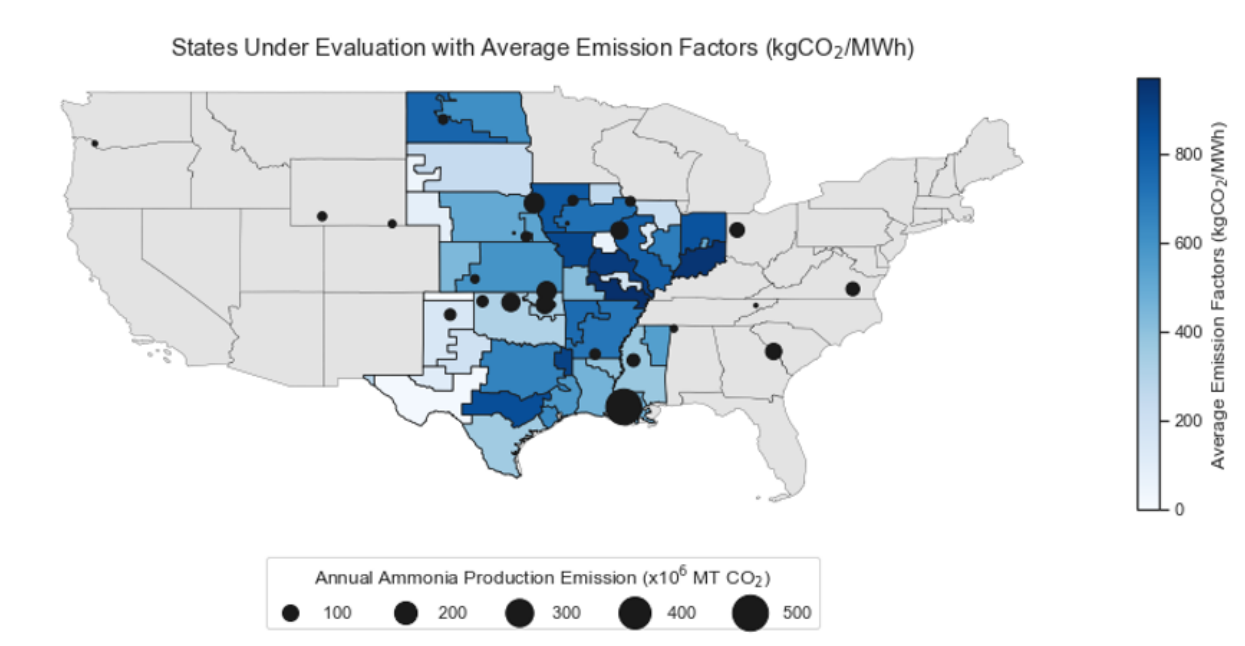

Figure 2: Time-average of marginal CO_2 emissions intensity for 2030 projected by National Renewable Energy Laboratory's analysis under mid-range renewables cost assumptions[48] for focus area of study. Reported average emissions intensity calculated as a simple average of hourly long-term marginal emissions factors reported for 8760 hours of the year. Major ammonia production facilities shown for reference, with the size of the bubble proportional to their annual CO_2 emissions in 2019[51]

Results and discussion

Operational Dynamics of electricity driven ammonia production

We highlight the functionalities of the developed integrated design and operations model by discussing the model outcomes for two locations in the United States - first (A) Amarillo, TX and second (B) Greenfield, IN - based on the above-mentioned 2030 technology cost assumptions and under scenarios with and without use of 2030 grid electricity conditions. The 2020-21 cost of natural gas-based ammonia is around 0.4 \$/kg,[52] while the levelized cost of ammonia (LCOA)[1] of the grid only case is 0.5-0.6 \$/kg and the completely VRE driven case

[1]LCOA = (Annualized CAPEX + OPEX)/ Yearly $NH_3 Production$

(VRE only) is between 0.95-1.20 $/kg at 2030 cost scenarios for the locations being evaluated (Figure 3). Based on simulated 2030 electricity prices and marginal emissions factors for the two locations, grid-electricity derived ammonia production has a positive abatement cost of 85 $/tonne CO_2 and corresponds to 77% CO_2 emissions reduction in Amarillo, TX, while it has a negative abatement cost (-28 $/tonne CO_2) and leads to 340% greater CO_2 emissions in Greenfield, IN. Here, the cost of carbon abatement(CoCA) is calculated via Eq. 1 ,where LCOA and CO_2 emissions intensity of the incumbent natural gas process and emissions intensity are assumed to be 0.4 $/kg and 2.35 tonnes CO_2/tonne NH_3.[5] Here, we do not include upstream emissions associated with the natural gas supply chain, that if included, would further lower the CO_2 abatement costs estimated here.

$$CoCA = (LCOA_{Process} - LCOA_{incumbent})/(Emissions_{incumbent} - Emissions_{Process}) \quad (1)$$

Thus, while it is possible to realize 80% CO_2 emission intensity reduction at a location with a low-emissions intensity grid (average grid emissions intensity at Amarillo, TX = 50 kgCO_2/MWh), connecting to a high emission grid (average grid emissions intensity at Greenfield, IN = 856 kgCO_2/MWh) results in higher emissions per tonne of ammonia and becomes a counter-productive solution in this case. 100% process CO_2 emissions removal is achievable at the two locations using VRE electricity supply and corresponds to a CO_2 abatement costs of 242 $/tonne CO_2 and 342 $/tonne CO_2 based on dedicated VRE electricity supply for the locations in TX and IN, respectively.

In addition to the levelized cost comparisons for these scenarios, the developed model provides detailed information of the investment requirements for each of the components in the facility (Figure SI 4) as well as the temporal dynamics of the system operation in response to electricity supply variability. We simulate the operations of the facility to run at constant production flow rate, which results in a constant baseline power input for operating the H-B

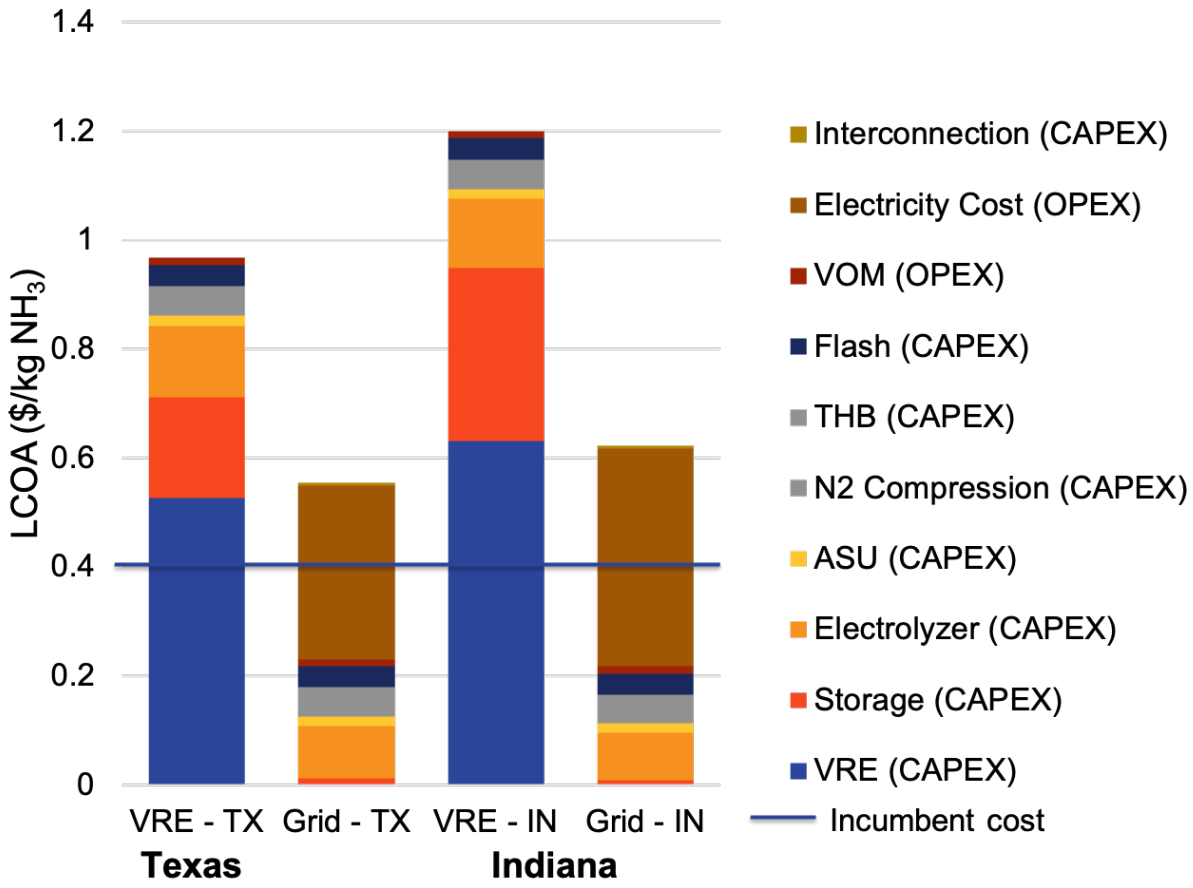

Figure 3: Levelized cost of ammonia (LCOA) comparison for VRE & Grid driven ammonia production for sample locations in Texas (near Amarillo, TX) and Indiana (Greensfield, IN). Grid supply modeled as per 2030 grid scenarios available from NREL Standard Scenarios.[48] Storage cost includes levelized cost of 3 types of storage - Li-ion battery, hydrogen storage (above ground) and nitrogen storage - see Figure SI 3 for details. Typical cost of natural gas based ammonia production in the US is shown as a horizontal line
. ASU = Air Separation Unit, VRE = Variable Renewable Electricity, THB = Thermochemical Haber-Bosch Synthesis loop, VOM = Variable operating and maintenance cost.

synthesis loop as well as constant flow of the reactants into the H-B synthesis loop. Figure 4 highlights the operation of VRE electricity-based plant, located in Amarillo, TX under low VRE availability periods (hours 25-65). During these periods, the majority of energy intensive and flexible processes (H_2 generation through electrolyzer and ASU are turned down/off(Figure 4(a)) while discharging from physical storage (Figure 4 (b,c)). Without grid connection, Li-ion battery storage is the only feasible option to provide the baseline power requirement for the base H-B synthesis loop and ammonia liquefaction (flash) during low VRE availability periods and contributes a 5-7% of total ammonia cost in both Texas and Indiana locations. Because of the availability of other lower cost forms of storage, Li-ion storage is not used for managing the seasonal variations in VRE supply.

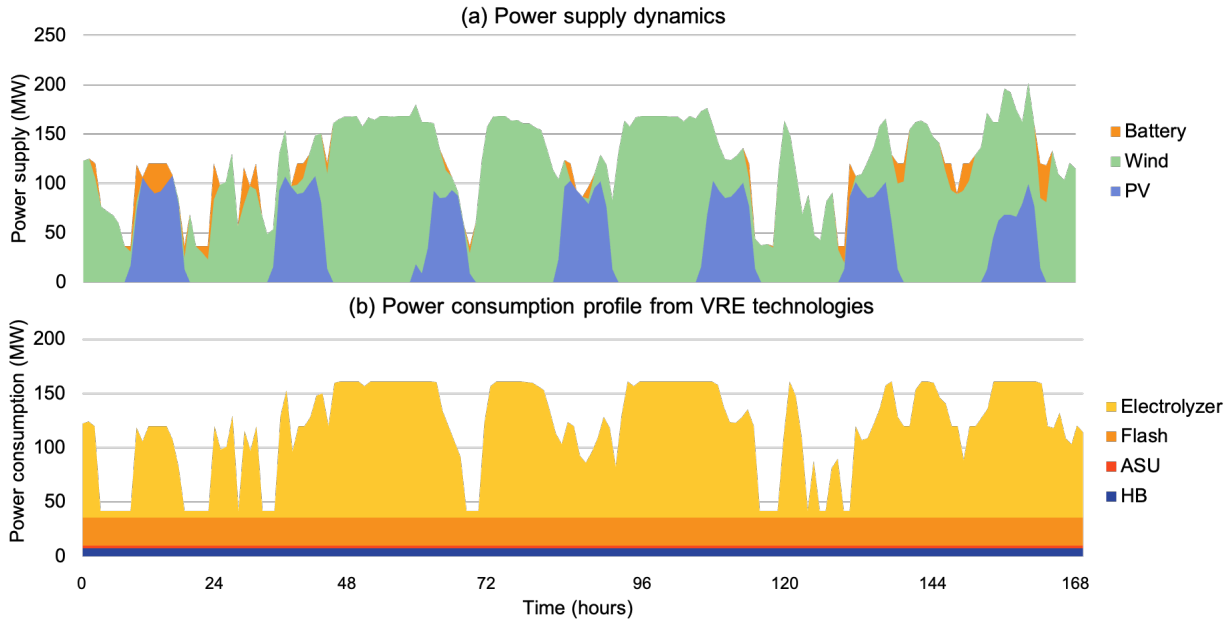

Figure 4: Plant operation over a representative week for VRE-based ammonia production facility in Amarillo, TX. (a) Power supply dynamics (b) Power consumption profile from VRE technologies

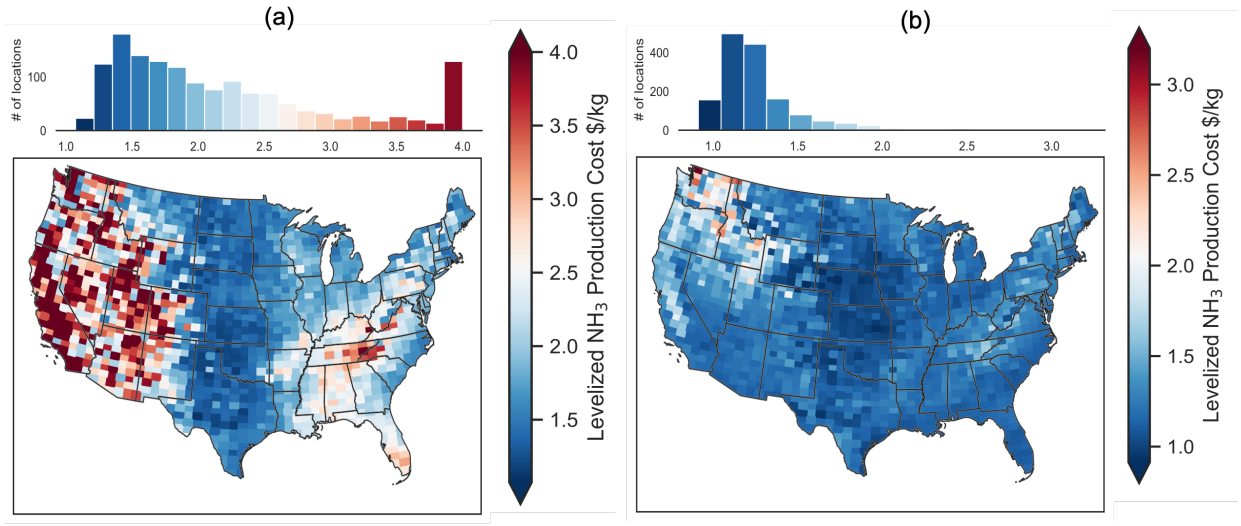

Figure 5: Spatial distribution in the levelized cost of ammonia map for (a) Wind driven (left) - 5^{th}, median and 95^{th} percentile CO_2 abatement cost : 343, 665, 1873 \$/tonne CO_2 (b) Wind + PV driven Electrolytic ammonia production (right) - 5^{th}, median and 95^{th} percentile CO_2 abatement cost : 260, 340, 596 \$/tonne CO_2

Estimated costs for dedicated VRE-based ammonia production in the United States

We evaluate the outcomes for both standalone solar(PV) and onshore wind driven ammonia production for continental U.S., and find that the resulting LCOA distributions largely follow spatial patterns in VRE resource availability owing to the dominant role of VRE capital cost in LCOA (results for PV only based facility configurations shown in Figure SI 5). For PV only systems, the key areas which provide the lowest LCOA are in southwest U.S. These regions, however, lack existing agricultural demand for ammonia (as inferred by location of existing ammonia production facilities), and may also lack access to freshwater, which might limit their deployment value. At the same time, for the emerging uses of ammonia as an energy carrier or fuel, these regions could be favored to serve neighboring demand centers such as California or the Gulf of Mexico region, wherein water needs could be met using relatively inexpensive reverse osmosis of sea water[53]. In case of wind-driven ammonia production (Figure 5a), the lowest cost regions better align with existing ammonia consumption regions, primarily the U.S Midwest, which accounts for more than 90% of the

ammonia production capacity in the country (Figure 2) . The costs of wind driven ammonia across the U.S. ranges from 1-12 $/kg ($5^{th}$, median, and 95^{th} percentile costs of 1.28 $/kg, 1.96 $/kg and 4.80 $/kg respectively) with about 93% of locations with a cost of less than 4 $/kg (more than 10x the cost of current fossil fuel driven ammonia production). Our modeling also reveals the distinctive dynamics and investment decisions driving the levelized cost outcomes for wind and PV driven systems. On comparing high wind (NE) and PV (AZ) resource quality with similar LCOA ($\sim$ \$1.04/kg), installed VRE capacity is almost twice as high for PV than wind given lower capacity factor of solar resources. For the same reasons, the intermediate storage options (Li-ion, H_2 and N_2) are relatively smaller (around 10% lower) for wind sites along with a higher capacity utilization of the electrolyzer (60% capacity factor for lowest cost wind site vs 32% for lowest cost PV site) (See Figure SI 6).

Figure 5(b) highlights how allowing for PV and wind resources to be used jointly results in lowering the cost of dedicated VRE-based ammonia production with a median cost of 1.20$/kg and 5^{th} and 95^{th} percentile of 1.01 and 1.80 $/kg, respectively. In fact, costs below 1 $/kg levels are estimated for 4% (58 out of 1487) of locations in the continental U.S. The complementary resource profiles for wind and PV led to reduced need for daily storage requirements for the on-site production facility (see Figure SI 6). While there is still a need for round-the-clock electricity supply to operate the inflexible H-B synthesis loop which necessitates the deployment of Li-ion battery storage, the battery capacity required is reduced with simultaneous wind and PV utilization (Figure SI 6). On average, battery energy capacity reduces by 10% for the locations with less than $ 1/kg NH_3 identified in 5(b) as compared to the wind only cases in 5(a). At each location, the relative contribution of wind and solar to the electricity supply capacity is dependent on dominant VRE resource in terms of resource quality for the region (Figure SI 7).

Carbon footprint and cost of ammonia production using grid + VRE electricity

The above analysis indicates that while dedicated VRE-based ammonia production can achieve full decarbonization, it is estimated to be more expensive than reliance on grid electricity-based supply even with 2030 technology cost assumptions that assume continued cost declines from 2020 cost levels. Moreover, as the CO_2 emissions intensity of the electric grid is anticipated to decrease over time due to increasing VRE penetration, the relative CO_2 emissions benefits of pursuing dedicated VRE electricity supply vs. grid electricity use are likely to diminish while the cost differences will remain. To understand this trade-off further, we explore the LCOA and process design outcomes for ammonia production using grid+VRE electricity supply under various CO_2 price scenarios. As identified in the previous section, the key demand and supply hubs for ammonia currently are in the Midwestern states and Texas, and therefore we focus this part of our analysis on this region. To explore the cost and emissions trade-offs of increasing VRE supply, we evaluate model outcomes for this region under the four CO_2 price scenarios: no policy, low CO_2 price (10 \$/tonne CO_2), medium (50 \$/tonne CO_2) and high CO_2 price (100 \$/tonne CO_2). For the analysis, we model the grid in 2030 as per the standard scenario projections from NREL for price and marginal CO_2 emissions for the system.[49]

Figure 6 shows that under the no-policy scenario, grid connectivity leads to relatively small spatial differences in LCOA outcomes but significant spatial variations in CO_2 emissions intensity. For example, under the no carbon price scenario, ammonia production in Texas, North & South Dakota and Nebraska is estimated to have 60-80% lower carbon intensity than ammonia production in Indiana or Illinois (Figure 6B top left panel). A 50 \$/tonne CO_2 policy leads to greater role for VRE generation in electricity supply for ammonia production and leads to more spatially uniform CO_2 emissions intensity outcomes (Figure 6b bottom left panel), that are generally below that of natural gas-based ammonia production. This is achieved by deploying more on-site VRE capacity at previously high-emission loca-

tions that can displace electricity use during high marginal emission intensity time periods of the day.

In general, increasing VRE penetration in the electric grid tends to increase instances of low wholesale electricity prices due to the well-documented merit order effect.[54] Consequently, we find that locations with low emissions intensity grid supply, synonymous with greater share of grid-based VRE generation, tend to also have lower LCOA. This explains why locations such as West Texas, Oklahoma & Kansas with low marginal CO_2 emission intensity electricity supply tend to have lower LCOA compared to higher marginal CO_2 emissions intensity grid locations in Indiana and Illinois across all CO_2 price scenarios (Figure 6). This observation and our scenario results indicate that favorable locations for electricity-based ammonia production, both in terms of cost and emissions, may overlap for different carbon policy scenarios. An important caveat to this finding is the price-taker assumption implicit in our calculation that assumes the industrial process represents a relatively small electricity demand that and hence cannot influence electricity prices and marginal CO_2 emissions substantially.

Impact of process flexibility on cost of VRE-based ammonia production

As noted earlier, for dedicated VRE-based ammonia production, round-the-clock operation of the H-B synthesis loop requires continuous electricity supply that necessitates the need for deploying Li-ion battery storage. Here, we explore how innovations to introduce flexibility in the H-B synthesis loop operations can contribute towards lowering the cost of dedicated VRE-based ammonia production while still adhering to the same round-the-clock ammonia supply requirements. Specifically, we investigate the cost and design impacts of the following two modifications: a) allowing the H-B synthesis to function at outputs below its nameplate capacity while constraining its ramp rate (10% change from previous hourly production level) and b) allowing storage of produced ammonia to enable producing more than nameplate

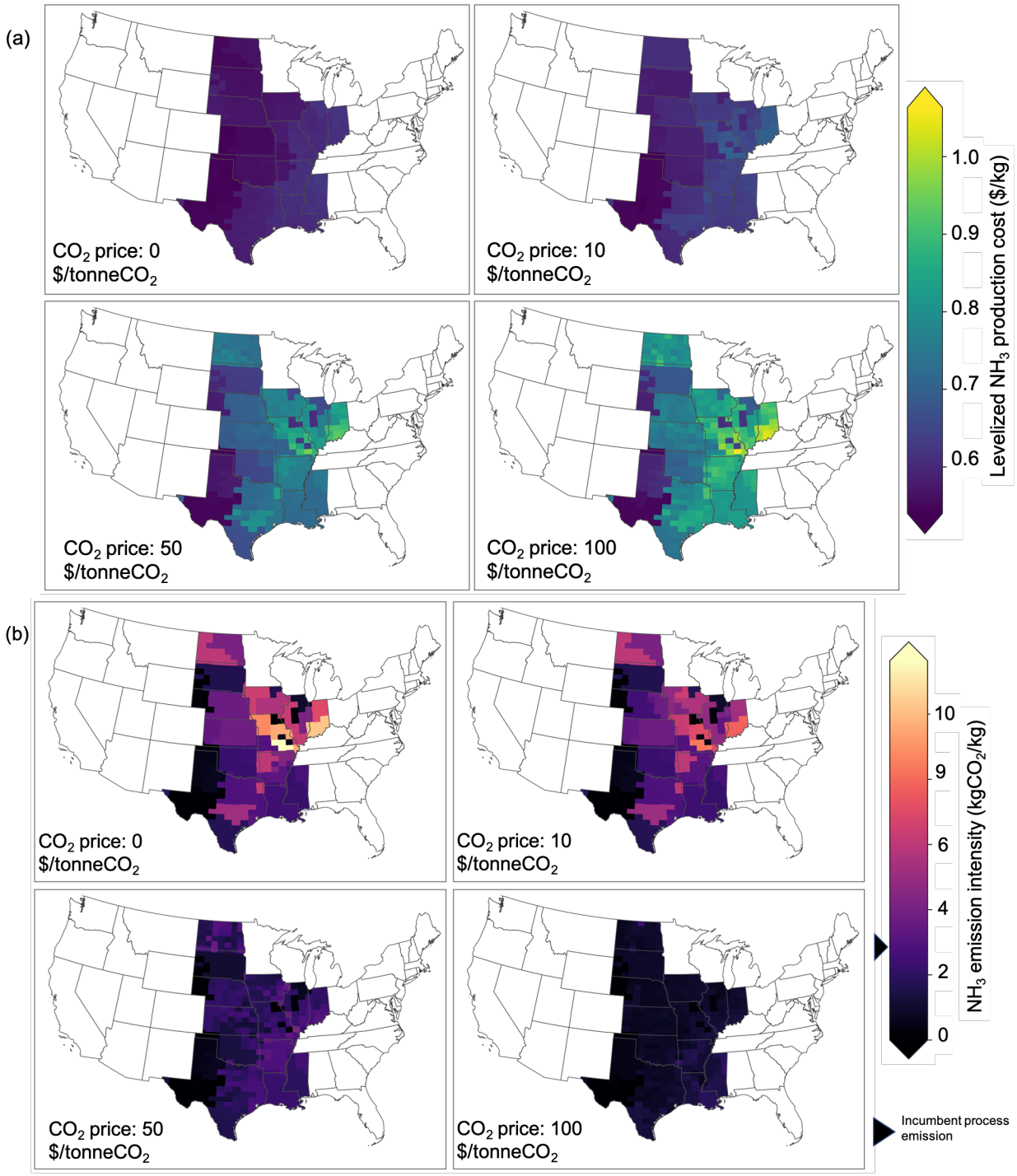

Figure 6: Spatial distribution in Levelized cost of ammonia (LCOA) (a) and average CO_2 emission intensity of ammonia production (b) for PV+wind + grid connected electrolytic ammonia production under different CO_2 price scenarios. Grid emissions and cost profiles for each location based on 2030 projections available from NREL standard scenarios modeling outcomes[48,49]

capacity at times of high VRE availability to make up for less than nameplate production at low VRE availability periods. We consider two forms of ammonia storage - large scale cryogenic ammonia storage at -33° C, 1 bar (larger than 20000 tonnes) and small scale high pressure storage systems (20 bar, 25 ° C). It should be noted that ammonia is still modeled to be output at a constant rate from the facility, which now can be supplied by a combination of ammonia storage and the H-B synthesis loop, since the produced ammonia might be used in other inflexible industrial processes (e.g. urea production).

Figure 7 highlights that introducing the specified flexibility in the H-B synthesis loop (e.g. ability to turn down by 50% or 75% compared to nameplate and stay at that level for 48 hours) can enable a 10-15% decline in LCOA compared to the case of an inflexible H-B synthesis loop. Figure 7 shows that the reduction in cost results from shifting the storage requirement downstream into the production process, with decreasing N_2 and H_2 storage and increasing NH_3 storage with increasing process flexibility. Moreover, the relative decrease in storage costs more than offsets the slight increase in cost of the H-B synthesis loop that needs to be oversized compared to the case of the inflexible process to enable NH_3 storage. In both the cases of flexible operations (50% and 75% flexibility cases), large scale cryogenic ammonia storage is selected with a capacity capable of providing more than 12-15 days of continuous ammonia output for the plant for the design capacity of the plant at 250 tonnes/day. Overall, this framework can be used to study the maximum affordable cost impacts of innovations to improve process flexibility that are valued in terms of improving the process economics.

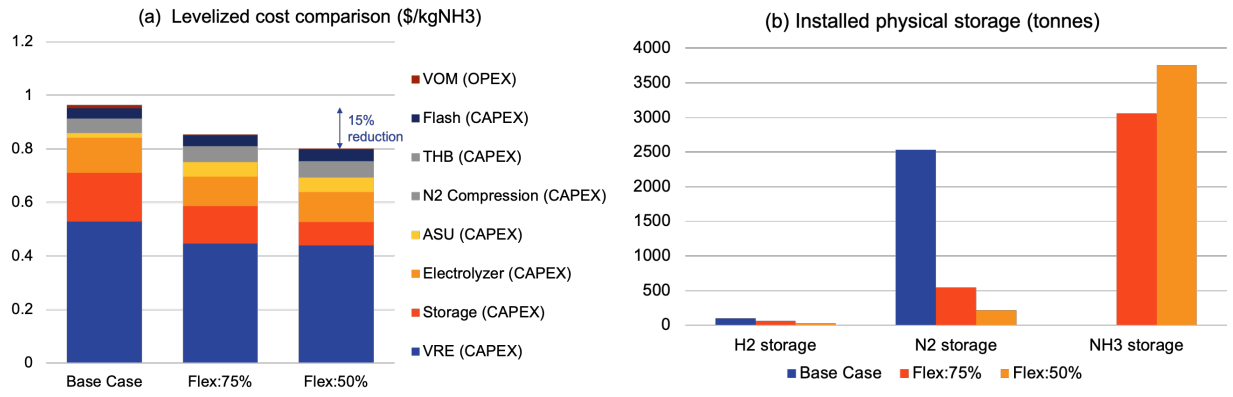

Figure 7: LCOA comparison for electricity-driven ammonia production with varying levels of flexibility for the thermochemical Haber-Bosch synthesis loop, ranging from no flexibility, H-B system turndown to 75 percent of design flow rate and system turndown to 50 percent of design flow rate (a), Storage Capacity installed for flexibility cases (b) (VOM : Variable Operation and Maintenance Cost, ASU : Air Separation Unit, VRE : Variable Renewable Energy, HB : Haber-Bosch Unit)

Conclusions

Here, we propose a systematic framework to explore the economics and CO_2 emissions impacts of commercially available electricity-driven ammonia production schemes while considering spatial and temporal variations in electricity supply from the grid as well as on-site production via VRE resources. Our findings are based on a design and operations modeling framework that allows for co-optimizing the size of various components, including grid connection, electricity, H_2, and N_2 generation capacity and different types of on-site storage while enabling round-the-clock, steady ammonia production. Based on 2030 technology cost and electric grid projections, we find that ammonia produced solely via grid electricity could achieve lower CO_2 emissions intensity as compared to natural gas based ammonia in some locations (e.g. Texas) but could also lead to higher CO_2 emissions intensity in other locations (E.g. Indiana) (CO_2 intensity of the grid drives which locations have higher or lower emissions). As illustrated elsewhere (Fig SI 8), the key drivers of the levelized cost is the cost of electricity - be it in the form of PV or Wind while variation in costs of other components such as electrolyzer or HB has lower impact on the LCOA. In contrast to grid

electricity use, dedicated wind- and solar PV-based ammonia production can reduce process CO_2 emissions by 100% but have widely different process designs and abatement costs depending on location, and configuration of VRE supply. Across the U.S., we investigated the cost of VRE-based electricity driven ammonia production and estimated the 5^th percentile, median and 95^th percentile values for resulting CO_2 abatement cost to be: 1) 343, 573, 984 \$/tonne CO_2 for PV –based electricity supply(LCOA: 1.21,1.74,2.71 \$/kg NH_3), 2) 376, 665, 1873 \$/tonne CO_2 for wind-based electricity supply (LCOA: 1.28,1.96,4.17 \$/kg NH_3) and 3) 260, 342, 596 \$/tonne CO_2 for PV+Wind based electricity supply (LCOA: 1.01,1.21,1.80 \$/kg NH_3). The combination of grid+co-located VRE electricity supply locations may be the most cost-effective way for reducing CO_2 emissions from ammonia production in the short-term since it reduces the on-site energy storage requirements for continuous ammonia production. In the midcontinental US states with existing agricultural ammonia demand, we find that 2030 grid + VRE connected ammonia under a \$50/tonne CO_2 policy scenario can achieve 55-100% CO_2 emissions reduction per tonne of ammonia produced compared to natural gas based routes, which corresponds to an abatement cost of 61 to 180 \$/tonne and LCOA of 0.54-0.63 \$/kg.

Finally, a key driver for cost of dedicated VRE systems is the need for battery storage to enable continuous power supply for the H-B synthesis loop and ammonia liquefaction systems. In this context, enabling operational flexibility in H-B synthesis to allow some ramping capability in ammonia production could be beneficial in reducing the cost of VRE-based ammonia supply. This analysis also suggests that emerging ammonia production routes based on electrochemical rather than thermochemical synthesis schemes that are likely to be more flexible, may be more synergistic and cost-effective for using VRE electricity input.

The methodological contributions of this paper in modeling the design and operation of electricity-driven chemical production can be extended to study other key industrial commodities with large carbon footprint like steel, cement, ethylene and methanol. In addition, there is scope for incorporating alternative technology choices for each of the system compo-

nents considered in the process, similar to the approach adopted by Palys and Daoutidis.[55] For instance, where feasible, utilization of underground hydrogen storage could be modeled with injection, withdrawal rates and pressurization requirements dependent on the location. For a given location, availability of underground H_2 storage, with lower capital cost per tonne than above-ground storage, could contribute towards reducing LCOA for VRE-only systems (see Figure SI 3 for H_2 storage cost contribution to LCOA).

The findings of this study should be interpreted keeping in mind the following limitations, which also are interesting areas of future work. First, our assessment of process and grid interactions are based on a price taker assumption that assumes no change in wholesale electricity prices or marginal grid emissions factors due to increasing grid electricity consumption by the ammonia production process. An interesting area of future work would be to represent such industrial electricity demand with flexibility constraints in grid operations models to understand the complete picture of large-scale electrification of industrial processes. Second, our spatial assessment of LCOA does not account for spatial variation in the cost of land or the cost of transporting ammonia from the production site to the point of consumption. The impact of ammonia shipping on the final landed costs can range from relatively small (5-7%)[2] for transport of the product in the continental US, but can be higher for trans-ocean shipments. Accounting for these attributes may lead to some locations being more favorable than others in terms of delivered cost of ammonia rather than LCOA metric used here. These factors could be included in a detailed supply chain analysis that also considers the capital cost differences between distributed and centralized ammonia production as well as alternate energy transport modes (electricity, ammonia) to connect energy production and consumption sites.

Third, our analysis relied on characterizing VRE resource availability based on a single weather year and while this is reasonable for a screening analysis, further assessment is needed to understand the impacts of inter-annual variability in VRE output as well as the impacts of climate change on VRE variability on LCOA of VRE-based ammonia production.

Fourth, while our analysis has quantified the potential benefits of process flexibility, further analysis using dynamic simulations is necessary to understand the operational implications of flexible process operation.

Acknowledgement

The authors thank Jack Morris at the MIT Energy Initiative for generating the renewable resource profiles for the various locations. A.B. acknowledges funding from the Energy Fellowship program at the MIT Energy Initiative. D.S.M acknowledges support from the low-carbon energy center on electric power systems at MIT Energy Initiative.

Supporting Information Available

SI 1. Additional model inputs

Renewable energy resource characterization

Hourly PV capacity factors (CF) are simulated using historical satellite-derived weather data from the National Solar Radiation Database (NSRDB)[56] as inputs to the open-source PVLIB model.[57] The native resolution of the NSRDB is 30min; modeled PV output is downsampled to hourly resolution using trapezoidal integration. All PV generators are assumed to employ horizontal single-axis tracking with a north-south axis of rotation (tracking from east to west throughout each day) and a DC-to-AC ratio of 1.3. Numerical assumptions (DC-to-AC ratio, system losses, temperature coefficient, etc.) are taken from Brown and Botterud[46] and generally match the assumptions used in the PVWatts model[58] and recent industry trends. PV capacity factors (CF) is simulated at an icosahedral mesh of sites spanning the continental U.S.

Hourly wind CF is simulated using historical meteorological data from the NREL Wind Integration National Dataset Toolkit (WTK)[59–62] and power curve data from commercial

wind turbines assuming a 100m hub height. We simulated wind resource output based on the Gamesa G26/2500 turbine power curve for the purpose of our study. A total of 42000 points in the continental U.S. was sampled which were then downsized to the 1487 points grid considered for our study by locating the points closest to the grid locations.

Cost assumptions

Table SI 1: Electrolyzer cost and design Parameters. Fixed Operations and Maintenance (FOM) costs noted here include the cost of periodic stack replacement, which explains why they are higher than estimated FOM cost in the literature.[63]

Parameter	Value	Units	Reference
Operating pressure	30	bar	
CAPEX	500	*$/kW*	[5]
Yearly FOM cost	5	*% of total capital cost*	[64]
Specific power consumption	53	*kWh/kg*	[5]
Minimum power load	5%	*% capacity*	[42]
Lifetime	20	*years*	
Water consumption	6.26	*gal/kgH2*	[65]

Table SI 2: Ammonia Synthesis and air separation unit Specific Parameters

Parameter	Value	Units	Reference
H-B Synthesis Unit	3,734,400	*$/(tonne/hr)*	[66]
H-B Unit Power Use	0.725	*MW/(tonne/hr)*	
PSA CAPEX			See Table SI 3
PSA Power Use	0.29	*MW/(tonne/hr)*	[33]

Table SI 3: PSA system - modelled CAPEX segments(LB = Lower bound, UB = Upper bound, Piece-wise Capex components modelled as upper(UB) and lower bounds(LB) of the segment)[33]

Segment	Capacity$_{LB}$ *tonne/hr*	Capacity$_{UB}$ *tonne/hr*	Capex$_{LB}$ *$*	Capex$_{UB}$ *$*
1	0	8.75	0	1,320,000
2	8.75	17.5	1,320,000	2,640,000
3	17.5	26.25	2,640,000	3,960,000
4	26.25	35	3,960,000	5,270,000
5	35	43.75	5,270,000	6,590,000

Table SI 4: Storage Costs & Operational Parameters

	Energy CAPEX	Power CAPEX	FOM Energy	FOM Power	Energy Units	Power Units	Reference
Li-ion Battery	116,000	101,000	2,987	2,240	MWh	MW	[47]
H2 Storage	345,000	1,200,000	3,450	48,000	tonne	tonne/hr	[67]
N2 Storage	1916	476,000	19	19,040	tonne	tonne/hr	[68]
NH3 Pressurized	5,058	60	50	0	tonne	tonne/hr	[69]
NH3 Cooled Storage	719	60	7	0	tonne	tonne/hr	[69]
Units	*$/Energy Unit*	*$/Power Unit*	*$/Energy Unit*	*$/Power Unit*			

SI 2. Additional Results

Electricity Price Map

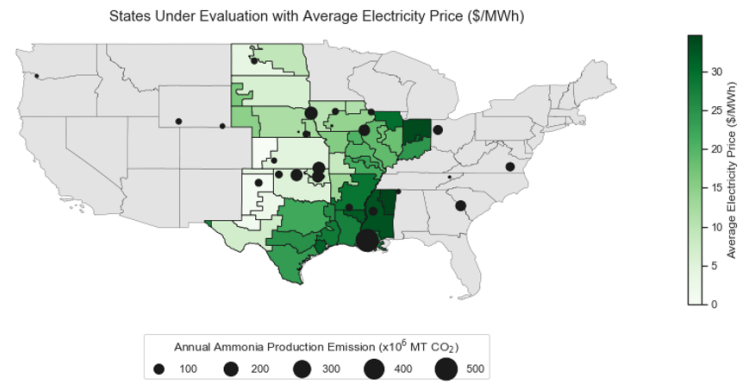

Figure SI 1: Average electricity price map for 2030 projected by National Renewable Energy Laboratory's analysis under mid-range renewable cost assumptions[48] for focus area of study. Major ammonia production facilities shown for reference, with the size of the bubble proportional to their annual CO_2 emissions (and production capacity) in 2019 locations[51]

VRE Resource Map

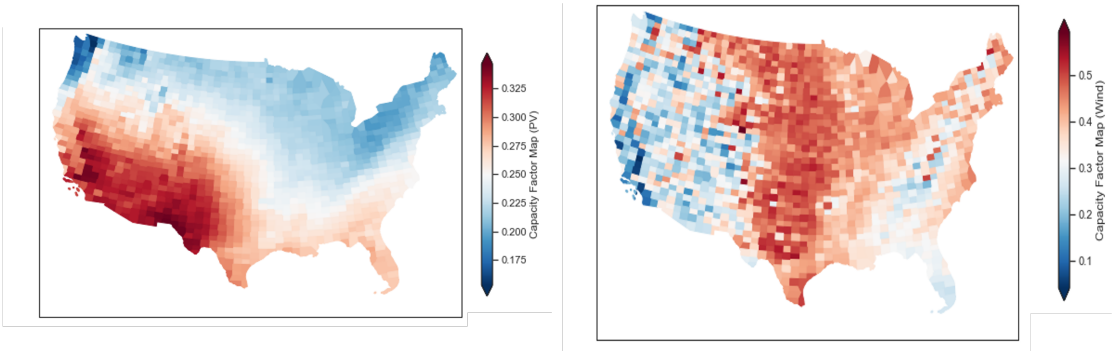

Figure SI 2: Average PV Capacity Factor (left), Average Wind Capacity Factor in continental US(right)

LCOA Comparison with storage cost contributons shown

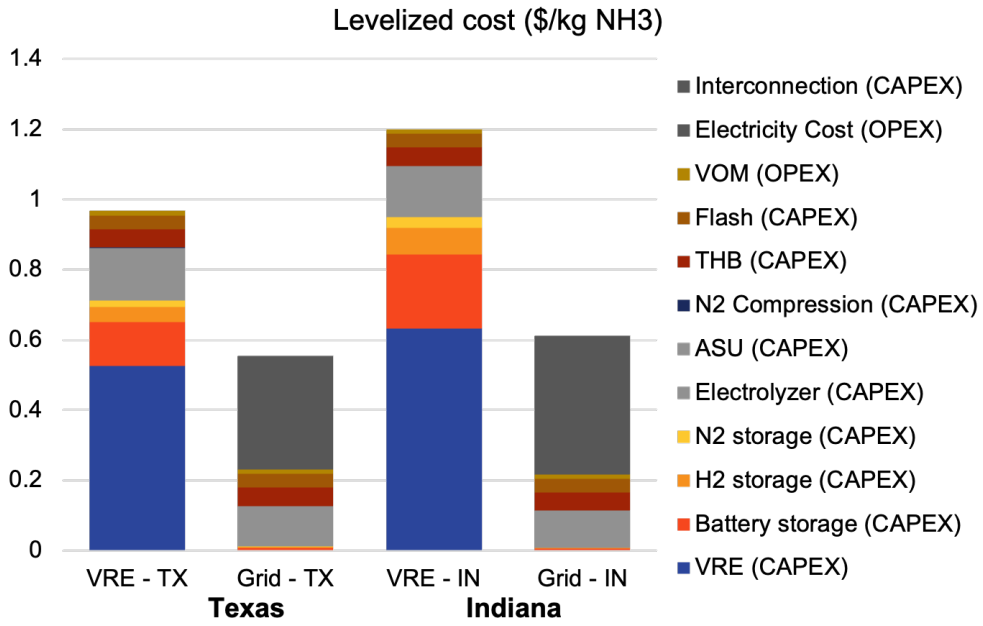

Figure SI 3: Levelized cost of ammonia production for locations : Amarillo, TX and Greenfield,IN with storage cost split

Infrastructure Deployment Mix for Base Case Model Runs

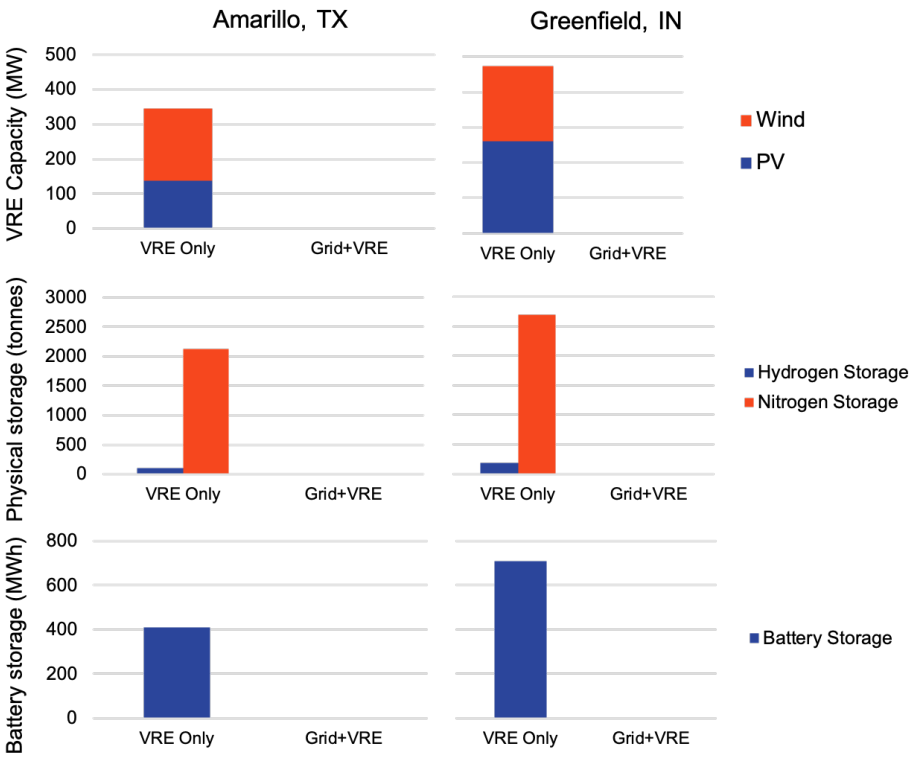

Figure SI 4: Investment Decisions for VRE and grid based Ammonia production for a sample location in West Texas(left) and Indiana(right)

LCOA Map - PV

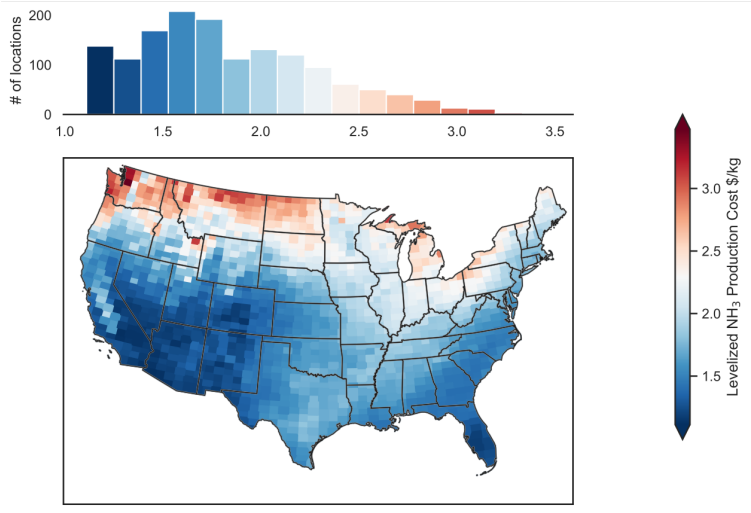

Figure SI 5: LCOA Map of PV only driven Ammonia production (5^th, median and 95^th percentile CO_2 abatement costs of 343, 573, 984 $/tonne CO_2)

PV & Wind System Design Comparison

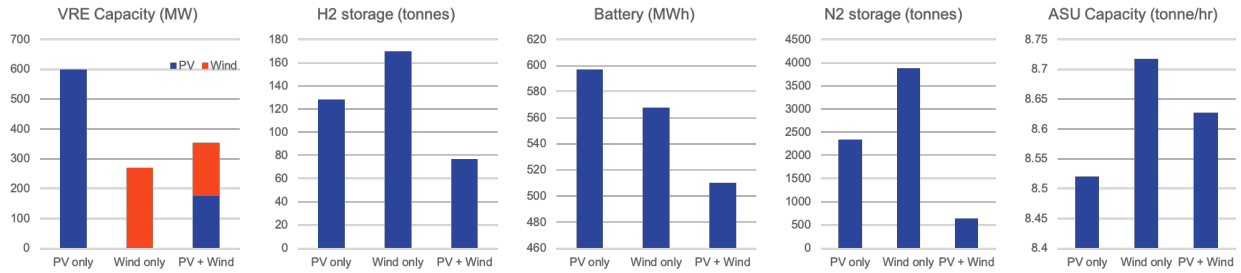

Figure SI 6: Comparison of individual system component sizing for the lowest LCOA locations for PV, Wind and hybrid PV + Wind based ammonia production systems (LCOA across locations in the range of 1-1.2$/kg)

Wind + PV Infrastructure Mix Ratio

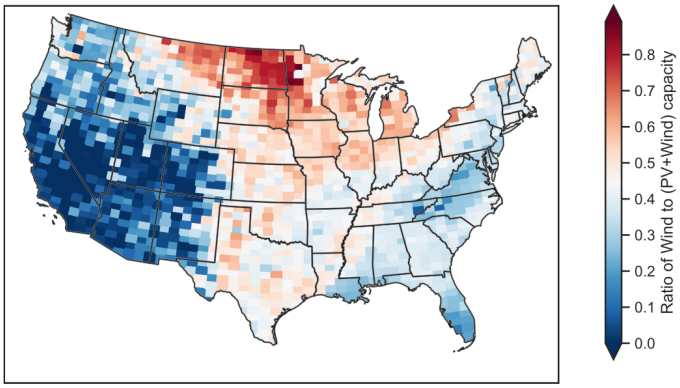

Figure SI 7: Ratio of Wind to total VRE Installed Capacity for combined Wind + PV deployment scenario

Sensitivity Analysis for Ammonia TEA Model

Figure SI 8 shows that the impact of lowering renewable electricity costs can have a great impact on changing the effective levelized cost of producing ammonia from the process envisioned here. As we have shown in the previous sections, the cost contribution of electricity-based ammonia production is dominated by VRE resource capital costs. A decline in the costs of the same or variation can have impacts as high as 40% on the currently estimated 2030 cost scenario.

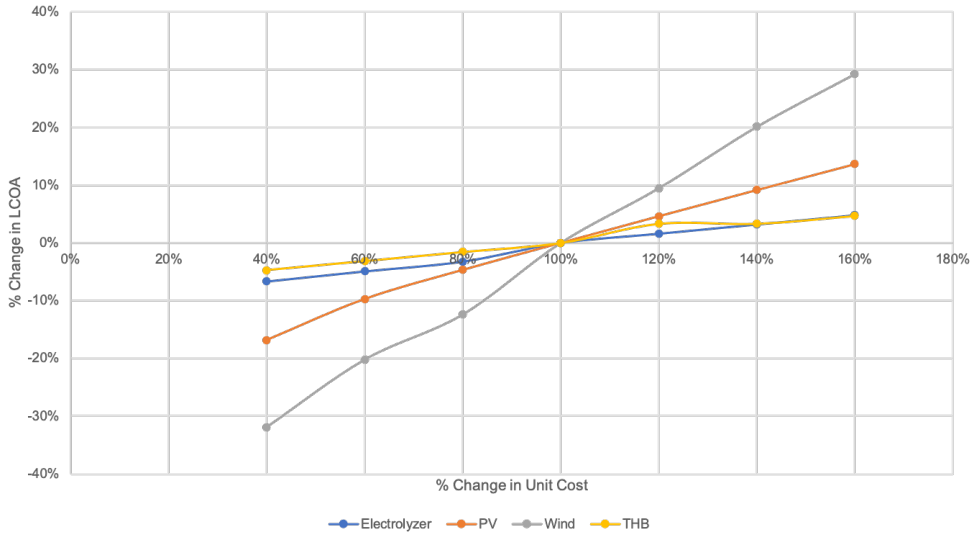

Figure SI 8: Impact of CAPEX variation for NH_3 synthesis process components (Analysis for location near Amarillo, TX - with inflexible HB system

SI 3. Ammonia model description

Table SI 5: Model Indices and Sets

Notation	Description
$t \in \mathcal{T}$	where t denotes a time step and $\mathcal{T}$ is the set of operational time steps modeled
$s \in \mathcal{S}$	type of storage technology
$\mathcal{S}^B \in \mathcal{S}$	where $\mathcal{S}^B$ set of electricity storage technologies with independent power (for both charge and discharge) and energy capacity variables
$\mathcal{S}^{N2} \in \mathcal{S}$	set of N_2 storage technologies with independently sized charging, discharging and energy capacity
$\mathcal{S}^{H2} \in \mathcal{S}$	set of H_2 storage technologies with independently sized charging (compression), discharging and energy capacity. Fixed cost of discharging capacity (e.g. pressure adjustment valve) is relatively minor and thus ignored here

$\mathcal{S}^{NH3} \in \mathcal{S}$	set of NH_3 storage technologies with independently sized charging (compression), discharging and energy capacity. Fixed cost of discharging capacity is relatively minor and thus ignored here
$g \in \mathcal{G}$	set of generation technologies which includes grid imports and variable renewable generators
$\mathcal{GR} \in \mathcal{G}$	grid electricity supply
$\mathcal{VRE} \in \mathcal{G}$	set of variable renewable generation technologies
$k \in \mathcal{K}$	set of piece-wise linear segments for modeling capital cost of air separation unit
$a \in \mathcal{ASU}$	set of air separation technologies
$e \in \mathcal{E}$	set of electrolyzer technologies
$r \in \mathcal{HB}$	set of Haber-Bosch ammonia synthesis reactor configurations
$f \in \mathcal{LIQ}$	set of ammonia separation technologies

Table SI 6: Decision Variables

Notation	**Description**
$\Omega_y^G \in \mathbb{R}_+$	Installed generation (or interconnection) capacity of technology $y \in \mathcal{VRE}$ (or $y \in \mathcal{GR}$) [MW]
$\Omega_y^E \in \mathbb{R}_+$	Installed energy storage capacity of technology $y \in \mathcal{S}$ [MWh for $y \in \mathcal{S}^B$ or tonnes if $y \in \mathcal{S}^{H2} \cup \mathcal{S}^{N2} \cup \mathcal{S}^{NH3}$]
$\Omega_y^C \in \mathbb{R}_+$	Installed charging capacity of technology $y \in \mathcal{S}$ - for $y \in \mathcal{S}^B$, charging and discharging capacity are set to be equal [MW for $y \in \mathcal{S}^B$ or tonnes/hour if $y \in \mathcal{S}^{H2} \cup \mathcal{S}^{N2} \cup \mathcal{S}^{NH3}$]
$\Omega_y^D \in \mathbb{R}_+$	Installed discharging capacity of technology $y \in \mathcal{S}^{N2}$ [tonnes/hour]
$\Omega_y^{ELY} \in \mathbb{R}_+$	Installed electrolyzer capacity of technology $y \in \mathcal{E}$ [MW]

$\Omega_y^{HB} \in \mathbb{R}_+$	Installed Haber-Bosch synthesis loop capacity of type $y \in \mathcal{HB}$ [tonne/hour]
$\Omega_y^{LIQ} \in \mathbb{R}_+$	Installed ammonia liquefaction capacity of type $y \in \mathcal{LIQ}$ [$MW_{thermal}$]
$\Omega_y^{ASU} \in \mathbb{R}_+$	Installed air separation unit capacity loop capacity of type $y \in \mathcal{ASU}$ [tonne/hour]
$x_{a,k} \in \mathbb{R}_+$	fractional value between 0 and 1 used to define cost and capacity of air separation unit $a \in \mathcal{ASU}$ in the piece-wise linear segment $k \in \mathcal{K}$
$w_{a,k} \in \{0,1\}$	binary variable used to define the active piece-wise linear segment $k \in \mathcal{K}$ that is used to compute the cost and capacity of air separation unit $a \in \mathcal{ASU}$
$\Pi_{a,t}^{ASU} \in \mathbb{R}_+$	Power consumed by air separation unit $a \in \mathcal{ASU}$ in time t [MW]
$\Pi_{e,t}^{ELY} \in \mathbb{R}_+$	Power consumed by electrolyzer $e \in \mathcal{ELY}$ in time t [MW]
$\Pi_{h,t}^{HB} \in \mathbb{R}_+$	Power consumed by electrolyzer $h \in \mathcal{HB}$ in time t [MW]
$\Pi_{s,t}^{C} \in \mathbb{R}_+$	Power (or mass flow rate) consumed by charging storage technology of type $s \in \mathcal{S}^B$ ($s \in \mathcal{S}^{H2} \cup \mathcal{S}^{N2} \cup \mathcal{S}^{NH3}$) in time t [MW (or tonne/hour)]
$\Pi_{f,t}^{F} \in \mathbb{R}_+$	Power consumed by NH3 liquefaction technology of type $f \in \mathcal{LIQ}$ in time t [MW]
$\Theta_{g,t}^{G} \in \mathbb{R}_+$	Power supplied by resource $g \in \mathcal{G}$ in time t [MW]
$\Theta_{s,t}^{D} \in \mathbb{R}_+$	Power (or mass flow rate) supplied by discharging storage technology of type $s \in \mathcal{S}^B$ ($s \in \mathcal{S}^{H2} \cup \mathcal{S}^{N2} \cup \mathcal{S}^{NH3}$) in time t [MW (or tonne/hour)]
$\Lambda_{e,t}^{E} \in \mathbb{R}_+$	H2 flow rate from electrolyzer $e \in \mathcal{ELY}$ in time t [tonne/hr]
$\Lambda_{e,h,t}^{EtoHB} \in \mathbb{R}_+$	H2 flow rate to NH3 synthesis loop $h \in \mathcal{HB}$ from electrolyzer $e \in \mathcal{ELY}$ in time t [tonne/hr]
$\Lambda_{e,s,t}^{EtoS} \in \mathbb{R}_+$	H2 flow rate to H2 storage $s \in \mathcal{S}^{H2}$ from electrolyzer $e \in \mathcal{ELY}$ in time t [tonne/hr]
$\Lambda_{a,t}^{ASU} \in \mathbb{R}_+$	N2 flow rate from air separation unit $a \in \mathcal{ASU}$ in time t [tonne/hr]

$\Lambda_{a,h,t}^{ASUtoHB} \in \mathbb{R}_+$	N2 flow rate from air separation unit $a \in \mathcal{ASU}$ to ammonia synthesis loop $h \in \mathcal{HB}$ in time t [tonne/hr]
$\Lambda_{a,s,t}^{ASUtoS} \in \mathbb{R}_+$	N2 flow rate from air separation unit $a \in \mathcal{ASU}$ to storage loop $s \in \mathcal{S}^{N2}$ in time t [tonne/hr]
$\Lambda_{h,t}^{HB} \in \mathbb{R}_+$	NH3 output flow rate from Haber-Bosch ammonia synthesis loop $h \in \mathcal{HB}$ in time t [tonne/hr]
$\Lambda_{h,s,t}^{HBtoS} \in \mathbb{R}_+$	NH3 output flow rate from Haber-Bosch ammonia synthesis loop $h \in \mathcal{HB}$ to NH3 storage $s \in \mathcal{S}^{NH3}$ in time t [tonne/hr]
$\Lambda_{h,t}^{HBtoOut} \in \mathbb{R}_+$	NH3 output flow rate from Haber-Bosch ammonia synthesis loop $h \in \mathcal{HB}$ to export in time t [tonne/hr]
$v_t^{plant} \in \{0,1\}$	Commitment state of the entire ammonia production facility at time t [-]
$v_{h,t}^{HB} \in \{0,1\}$	Commitment state of the Haber-Bosch Synthesis Loop h at time t [-]
$v_{h,t}^{ELY} \in \{0,1\}$	Commitment state of the electrolyzer h at time t [-]
$\chi_t^{plant} \in \{0,1\}$	binary variable indicating startup of entire ammonia production facility at time t [-]
$\chi_{h,t}^{HB} \in \{0,1\}$	binary variable indicating startup of Haber-Bosch Synthesis Loop h at time t [-]
$\zeta_t^{plant} \in \{0,1\}$	binary variable indicating shutdown of entire ammonia production facility at time t [-]
$\zeta_{h,t}^{HB} \in \{0,1\}$	binary variable indicating shutdown of Haber-Bosch Synthesis Loop h at time t [-]
$\Gamma_{s,t} \in \mathbb{R}_+$	state of charge of storage of type $s \in \mathcal{S}$ at time t [MWh or tonnes]

Table SI 7: Parameters

Notation	**Description**

$\pi_y^{I,G}$	Annualized capital cost of power generator $y \in \mathcal{G}$ - for $y \in \mathcal{GR}$, this corresponds to interconnection cost, while for $y \in \mathcal{VRE}$ this is an investment cost [$/MW/year]
$\pi_y^{I,ELY}$	Annualized capital cost of electrolyzer $y \in \mathcal{ELY}$ [$/MW/year]
$\overline{\pi}_{y,k}^{I,ASU}$	Annualized capital cost of air separation unit $y \in \mathcal{ASU}$ for upper capacity limit of piece-wise linear segment $k \in \mathcal{K}$ [$/year]
$\underline{\pi}_{y,k}^{I,ASU}$	Annualized capital cost of air separation unit $y \in \mathcal{ASU}$ for lower capacity limit of piece-wise linear segment $k \in \mathcal{K}$ [$/year]
$\pi_y^{I,HB}$	Annualized capital cost of Haber-Bosch Synthesis loop $y \in \mathcal{HB}$ [$/(tonne/hour)/year]
$\pi_y^{I,LIQ}$	Annualized capital cost of NH3 liquefaction loop $y \in \mathcal{LIQ}$ [$/$MW_{thermal}/year$]
π_y^{I,S^C}	Annualized capital cost of storage charging $y \in \mathcal{S}$ [$/MW/year if $yin\mathcal{S}^B$ else $/(tonne/hour)/year]
π_y^{I,S^E}	Annualized capital cost of energy capacity of storage $y \in \mathcal{S}$ [$/MWh/year if $yin\mathcal{S}^B$ else $/(tonne/year]
π_y^{I,S^D}	Annualized capital cost of storage discharging $y \in \mathcal{S}^{N2}$ [$/(tonne/hour)/year]
$\pi_y^{F,G}$	fixed operation and maintenance (FOM) cost of power generator $y \in \mathcal{G}$ [$/MW/year]
$\pi_y^{F,ELY}$	FOM cost of electrolyzer $y \in \mathcal{ELY}$ [$/MW/year]
$\pi_y^{F,HB}$	FOM cost of Haber-Bosch Synthesis loop $y \in \mathcal{HB}$ [$/(tonne/hour)/year]
$\pi_y^{F,LIQ}$	FOM cost of NH3 liquefaction loop $y \in \mathcal{LIQ}$ [$/$MW_{thermal}/year$]
π_y^{F,S^C}	FOM cost of storage charging $y \in \mathcal{S}$ [$/MW/year if $yin\mathcal{S}^B$ else $/(tonne/hour)/year]
π_y^{F,S^D}	FOM cost of storage discharging $y \in \mathcal{S}^{N2}$ [$/(tonne/hour)/year]

π_y^{V,S^D}	Variable cost of storage discharging $y \in \mathcal{S}$ [\$/MWh if $y \in \mathcal{S}^B$ else \$/(tonne)]
$\pi_y^{V,ELY}$	Variable cost of electrolyzer $y \in \mathcal{ELY}$ - includes cost of feed water supply[\$/MWh]
$\pi_y^{V,HB}$	Variable cost of Haber-Bosch Synthesis loop $y \in \mathcal{HB}$ - includes cost of cooling water supply and catalyst replacement cost [\$/(tonne)]
$\rho_{y,t}^{price}$	price of electricity supply from resource $y \in \mathcal{GR}$ at time t [\$/MWh]
$\rho_{y,t}^{MEF}$	marginal CO_2 emissions intensity of electricity supply from resource $y \in \mathcal{GR}$ at time t [tonnes CO_2/MWh]
$\rho_{y,t}^{CF}$	capacity factor of electricity supply from resource $y \in \mathcal{VRE}$ at time t [-]
α^{CO2}	CO_2 emissions penalty [\$/tonne CO_2]
$\overline{\Delta}_{y,k}^{ASU}$	Upper bound of installed capacity of air separation unit $y \in \mathcal{ASU}$ for piece-wise linear segment $k \in \mathcal{K}$ for [tonne / hour]
$\underline{\Delta}_{y,k}^{ASU}$	Lower bound of installed capacity of air separation unit $y \in \mathcal{ASU}$ for piece-wise linear segment $k \in \mathcal{K}$ for [tonne / hour]
β_y^C	Electricity requirement associated with charging storage of type $y \in \mathcal{S}^{H2} \cup \mathcal{S}^{N2} \cup \mathcal{S}^{NH3}$ [MWh/tonne]
β_y^D	Electricity requirement associated with discharging storage of type $y \in \mathcal{S}^{N2}$ [MWh/tonne]
β_y^{ASU}	Electricity requirement associated with air separation unit of type $y \in \mathcal{ASU}$ [MWh/tonne]
β_y^{ELY}	Electricity requirement associated with electrolyzer of type $y \in \mathcal{ELY}$ [MWh/tonne]
β_y^{HB}	Electricity requirement associated with H-B synthesis loop of type $y \in \mathcal{HB}$ [MWh/tonne]
β_y^{LIQ}	Electricity requirement associated with NH3 separation/liquefaction of type $y \in \mathcal{LIQ}$ [MWh/tonne]

τ^{ops}	Number of operating times steps, which is equivalent to index of last operating time step of the year [hours]
τ^{plant}	minimum plant downtime period [hours]
τ^{HB}	minimum Haber-Bosch Synthesis loop downtime period [hours]
$\alpha^{NH3Flow}$	Design flow rate for the NH3 production facility [tonne/hour]
$\alpha^{plantavail}$	Annual plant availability factor [hours/year]
η_s^C	Charging efficiency of storage of type $s \in \mathcal{S}$
η_s^D	Discharging efficiency of storage of type $s \in \mathcal{S}$
$\rho_h^{min,HB}$	Minimum production output of H-B synthesis loop as a fraction of nameplate capacity [-]
$\rho_h^{min,ELY}$	Minimum production output of electrolyzer as a fraction of nameplate capacity [-]
κ_h^{HB}	Hourly ramp rate of H-B synthesis loop output (upward and downward) as a fraction of nameplate capacity [-]
$\overline{\Omega}_h^{HB,ELY}$	Maximum capacity of Haber-Synthesis loop and Electrolyzer $h \in \mathcal{HB}, \mathcal{ELY}$ [tonne/hour]
$\underline{\Omega}_h^{HB,ELY}$	Minimum capacity of Haber-Synthesis loop and Electrolyzer $h \in \mathcal{HB}, \mathcal{ELY}$ [tonne/hour]

Objective function

The Objective Function(Eq. 2) minimizes sum of capital and operating costs of all units as shown below.

$$\sum_{y\in\mathcal{G}}\left((\pi_y^{I,G}+\pi_y^{F,G})\times\Omega_y^{G}\right)+\sum_{y\in\mathcal{ELY}}\left((\pi_y^{I,ELY}+\pi_y^{F,ELY})\times\Omega_y^{ELY}\right)+$$
$$\sum_{y\in\mathcal{LIQ}}\left((\pi_y^{I,LIQ}+\pi_y^{F,LIQ})\times\Omega_y^{LIQ}\right)+\sum_{y\in\mathcal{HB}}\left((\pi_y^{I,HB}+\pi_y^{F,HB})\times\Omega_y^{HB}\right)+$$
$$\sum_{y\in\mathcal{S}}\left((\pi_y^{I,S^C}+\pi_y^{F,S^C})\times\Omega_y^{C}\right)+\sum_{y\in\mathcal{S}}\left((\pi_y^{I,S^E}+\pi_y^{F,S^E})\times\Omega_y^{E}\right)+\sum_{y\in\mathcal{S}^{N2}}\left((\pi_y^{I,S^D}+\pi_y^{F,S^D})\times\Omega_y^{D}\right)+$$
$$\sum_{k\in\mathcal{K}}\sum_{a\in\mathcal{ASU}}\left(x_{a,k}\times(\underline{\pi}_{a,k}^{I,ASU}-\overline{\pi}_{a,k}^{I,ASU})+w_{a,k}\times\overline{\pi}_{a,k}^{I,ASU}\right)+$$
$$\sum_{y\in\mathcal{S}}\sum_{t\in\mathcal{T}}\left(\pi_y^{V,S^D}\times\Theta_{y,t}^{D}\right)+\sum_{y\in\mathcal{ELY}}\sum_{t\in\mathcal{T}}\left(\pi_y^{V,ELY}\times\Pi_{y,t}^{ELY}\right)+\sum_{y\in\mathcal{HB}}\sum_{t\in\mathcal{T}}\left(\pi_y^{V,HB}\times\Lambda_{y,t}^{HBtoProd}\right)+$$
$$\sum_{y\in\mathcal{GR}}\sum_{t\in\mathcal{T}}\left(\rho_{y,t}^{price}\times\Theta_{y,t}^{G}\right)+\sum_{y\in\mathcal{GR}}\sum_{t\in\mathcal{T}}\left(\rho_{y,t}^{MEF}\times\alpha^{CO2}\times\Theta_{y,t}^{G}\right)\tag{2}$$

System-level constraints

The power balance constraint of the model (Eq. 3) ensures that electricity demand and supply are in balance at each time step.

$$\sum_{y\in\mathcal{GR}}\Theta_{y,t}^{G}+\sum_{y\in\mathcal{VRE}}\Theta_{y,t}^{G}+\sum_{y\in\mathcal{S}^B}\Theta_{y,t}^{D}=$$
$$\sum_{y\in\mathcal{ELY}}\Pi_{y,t}^{ELY}+\sum_{y\in\mathcal{ASU}}\Pi_{y,t}^{ASU}+\sum_{y\in\mathcal{S}^B}\Pi_{y,t}^{C}+$$
$$\sum_{y\in\mathcal{HB}}\Pi_{y,t}^{HB}+\sum_{y\in\mathcal{LIQ}}\Pi_{y,t}^{LIQ}+\sum_{y\in\mathcal{S}^{H2}\cup\mathcal{S}^{N2}\cup\mathcal{S}^{NH3}}\left(\beta_y^{C}\times\Pi_{y,t}^{C}\right)+\Pi_{y,t}^{LIQ}+\sum_{y\in\mathcal{S}^{N2}}\left(\beta_y^{D}\times\Theta_{y,t}^{D}\right)\tag{3}$$

Eqn. 4 enforces that when the plant is online, the sum of ammonia exported from NH3 storage discharging and that exported to product from Haber-Bosch synthesis loop should equal the design flow rate,$\alpha^{NH3Flow}$. Eqns. 5 keeps track of when plant is online and online, with constraint for the first period of the year looking back at the plant status in the last

period (year length given by τ^{ops}) of the year. Eqn. 6 enforces minimum annual availability of plant operation, specified by $\alpha^{plantavail}$. Eqns. 7 enforces that when plant is shut down, it should remain shut down for at least τ^{plant} number of hours.

$$\sum_{h\in\mathcal{H}} \Lambda_{h,t}^{HBtoOut} + \sum_{s\in\mathcal{S}^{NH3}} \Theta_{s,t}^{D} = \alpha^{NH3Flow} \times v_t^{plant} \quad \forall t \in \mathcal{T} \tag{4}$$

$$v_t^{plant} = v_{t-1}^{plant} + \chi_t^{plant} - \zeta_t^{plant} \quad \forall t \in \{\mathcal{T}|t \neq 1\}$$

$$v_t^{plant} = v_{t+\tau^{ops}-1}^{plant} + \chi_t^{plant} - \zeta_t^{plant} \quad \forall t \in \{\mathcal{T}|t = 1\} \tag{5}$$

$$\sum_{t\in\mathcal{T}} v_t^{plant} = \alpha^{plantavail} \tag{6}$$

$$1 - v_t^{plant} \geq \sum_{r\in[t-\tau^{plant},t]} \zeta_r^{plant} \quad \forall t \in \{\mathcal{T}|t > \tau_{plant}\}$$

$$1 - v_t^{plant} \geq \sum_{r\in[1,t]} \zeta_r^{plant} + \sum_{r\in[\tau^{ops}-\tau^{plant}-t,\tau^{ops}]} \zeta_r^{plant}$$

$$\forall t \in \{\mathcal{T}|t \leq \tau_{plant}\} \tag{7}$$

Power supply and storage constraints

Eqns. 8 and 9 enforce capacity constraints on the supply of electricity from VRE and grid sources, respectively. Note that such a representation allows for VRE curtailment during periods of excess VRE availability. Eqn. 10 enforces storage inventory balance constraint for all storage technologies considered in the analysis. Eqn. 11 enforces the storage inventory cannot exceed installed storage capacity for all time periods. Eqn. 12 enforces that rate of charging and discharging on different storage technologies must adhere to their installed capacity limits. For battery storage, charging and discharging capacity are the same variable, while for nitrogen storage, charging and discharging are different decision variables. H2 and NH3 storage discharging rate is modeled to be unconstrained, given the relatively minor cost associated with these equipment (e.g. valves).

$$\Theta^G_{y,t} \leq \rho^{CF}_{y,t} \times \Omega^G_y \quad \forall g \in \mathcal{VRE}, \forall t \in \mathcal{T} \tag{8}$$

$$\Theta^G_{y,t} \leq \Omega^G_y \quad \forall g \in \mathcal{G}, \forall t \in \mathcal{T} \tag{9}$$

$$\Gamma_{s,t} = \Gamma_{s,t-1} + \eta^C \times \Pi^C_{s,t} - \frac{\Theta^D_{s,t}}{\eta^D} \quad \forall t \in \{\mathcal{T}/t > 1\}, s \in \mathcal{S}$$

$$\Gamma_{s,t} = \Gamma_{s,t+\tau^{ops}-1} + \eta^C_s \times \Pi^C_{s,t} - \frac{\Theta^D_{s,t}}{\eta^D_s} \quad \forall t \in \{\mathcal{T}/t = 1\}, s \in \mathcal{S} \tag{10}$$

$$\Gamma_{s,t} \leq \Omega^E_s \quad \forall s \in \mathcal{S}, t \in \mathcal{T} \tag{11}$$

$$\Pi^C_{s,t} \leq \Omega^C_s \quad \forall s \in \mathcal{S}, t \in \mathcal{T}$$

$$\Pi^D_{s,t} \leq \Omega^C_s \quad \forall s \in \mathcal{S}^B, t \in \mathcal{T}$$

$$\Pi^D_{s,t} \leq \Omega^D_s \quad \forall s \in \mathcal{S}^{N2}, t \in \mathcal{T} \tag{12}$$

Air separation unit

Eqn. 13 - 15 models the piece-wise linear segments used to compute the capital cost of the air separation unit. Eqn. 16 related electricity consumption of ASU with total N2 production rate, while Eqn. 17 enforces that total N2 product sent to H-B synthesis loop and N2 storage must equal the total N2 production rate from ASU at each time step.

$$\Omega^{ASU}_a = \sum_{k \in \mathcal{K}} \left(x_{a,k} \times (\underline{\alpha}^{ASU}_{y,k} - \overline{\Delta}^{ASU}_{a,k}) + w_{a,k} \times \overline{\Delta}^{ASU}_{a,k} \right) \quad \forall a \in \mathcal{ASU} \tag{13}$$

$$x_{a,k} \leq w_{a,k} \quad \forall a \in \mathcal{ASU}, k \in \mathcal{K} \tag{14}$$

$$\sum_{k \in \mathcal{K}} w_{a,k} = 1 \quad \forall a \in \mathcal{ASU} \tag{15}$$

$$\Pi^{ASU}_{a,t} = \beta^{ASU}_a \times \Lambda^{ASU}_{a,t} \quad \forall t \in \mathcal{T}, a \in \mathcal{ASU} \tag{16}$$

$$\Lambda^{ASU}_{a,t} = \sum_{h \in \mathcal{HB}} \Lambda^{ASUtoHB}_{a,h,t} + \sum_{s \in \mathcal{S}^{N2}} \Lambda^{ASUtoS}_{a,s,t} \quad \forall t \in \mathcal{T}, a \in \mathcal{ASU} \tag{17}$$

Electrolyzer

Eqn. 18 relates electrolyzer electricity consumption with total H_2 production rate, while Eqn. 19 enforces that total H_2 product sent to H-B synthesis loop and H_2 storage must equal the total N_2 production rate from electrolyzer at each time step.

$$\Pi_{y,t}^{ELY} = \beta_y^{ELY} \times \Lambda_{y,t}^{Ely} \quad \forall t \in \mathcal{T}, y \in \mathcal{ELY} \tag{18}$$

$$\Lambda_{y,t}^{ELY} = \sum_{h \in \mathcal{HB}} \Lambda_{a,h,t}^{EtoHB} + \sum_{s \in \mathcal{S}^{H2}} \Lambda_{a,s,t}^{EtoS} \quad \forall t \in \mathcal{T}, a \in \mathcal{ELY} \tag{19}$$

Eqns.20-21 models electrolyzer production capacity limits. The variable $\Omega_{h,t}^{ELY+}$ in the right hand of Eqn. 20-21 is a continuous variable, representing the product of the binary variable v_t^{ELY} and the continuous variable, Ω_h^{ELY}. This product cannot be defined explicitly, since it will lead to a bilinear expression involving two variables. Instead, we enforce this definition via the Glover's Linearization as per the set of constraints in Eqn. 22 (also referred McCormick Envelopes constraints for bilinear expressions, which is exact when one of the variables is binary). Finally, Eqn. 23 ensures that when the plant is offline, the electrolyzer is also offline.

$$\Lambda_{h,t}^{ELY} \leq \Omega_{h,t}^{ELY+} \quad \forall h \in \mathcal{ELY}, \forall t \in \mathcal{T} \tag{20}$$

$$\Lambda_{h,t}^{ELY} \geq \rho^{min,ELY} \times \Omega_{h,t}^{ELY+} \quad \forall h \in \mathcal{ELY}, \forall t \in \mathcal{T} \tag{21}$$

$$\begin{aligned}
&\Omega_{h,t}^{ELY+} \leq \overline{\Omega}_h^{ELY} \times v_{h,t}^{ELY} \quad \forall h \in \mathcal{ELY}, \forall t \in \mathcal{T} \\
&\Omega_{h,t}^{ELY+} \geq \underline{\Omega}_h^{ELY} \times v_{h,t}^{ELY} \quad \forall h \in \mathcal{ELY}, \forall t \in \mathcal{T} \\
&\Omega_{h,t}^{ELY+} \geq \Omega_h^{ELY} - \left(1 - v_{h,t}^{ELY}\right) \times \overline{\Omega}_h^{ELY} \quad \forall h \in \mathcal{ELY}, \forall t \in \mathcal{T} \\
&\Omega_{h,t}^{ELY+} \leq \Omega_h^{ELY} - \left(1 - v_{h,t}^{ELY}\right) \times \underline{\Omega}_h^{ELY} \quad \forall h \in \mathcal{ELY}, \forall t \in \mathcal{T}
\end{aligned} \tag{22}$$

$$v_{h,t}^{ELY} \leq v_t^{Plant} \quad \forall h \in \mathcal{ELY}, t \in \mathcal{T} \tag{23}$$

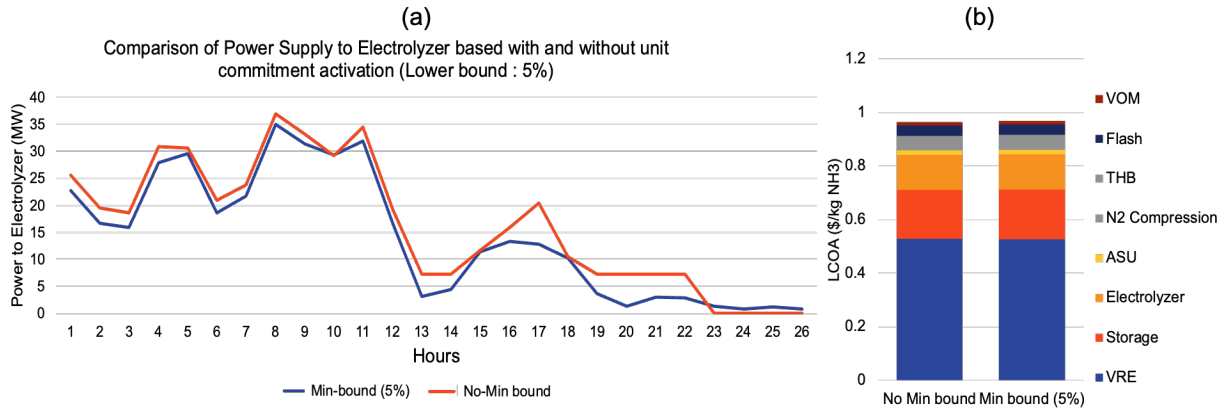

Figure SI 9: (a) Comparison of electrolyzer power input with and without non-zero power load (5%) for the electrolyzer. The effect of minimum load constraint on dispatch can be seen near hour 23 where the blue line is above the red line. (b) Impact of lower bound for electrolyzer power input on LCOA

Haber-Bosch synthesis

Eqn.24 - 25 enforces materials balances and stoichiometry of the net ammonia synthesis reaction occurring in the H-B synthesis loop. Here are we are modeling 100% conversion of the feed H2 and N2 into the H-B synthesis loop, which includes recycling of unconverted products from the reactor and associated recompression energy and costs - see Fig. SI 10 for the flowsheet of the synthesis loop modeled in Aspen Plus that is used to parametrize the energy (see Eqn. 26) and cost of the H-B synthesis loop in the optimization model.

$$\sum_{e \in \mathcal{ELY}} \Lambda_{e,h,t}^{EtoHB} = 3/14 \times \sum_{a \in \mathcal{ASU}} \Lambda_{a,h,t}^{ASUtoHB} \quad \forall h \in \mathcal{HB}, \forall t \in \mathcal{T} \tag{24}$$

$$\sum_{e \in \mathcal{ELY}} \Lambda_{e,h,t}^{EtoHB} + \sum_{a \in \mathcal{ASU}} \Lambda_{a,h,t}^{ASUtoHB} = \Lambda_{h,t}^{HB} \quad \forall h \in \mathcal{HB}, \forall t \in \mathcal{T} \tag{25}$$

$$\Pi_{h,t}^{HB} = \beta_h^{HB} \times \Lambda_{h,t}^{HB} \quad \forall h \in \mathcal{HB}, \forall t \in \mathcal{T} \tag{26}$$

Eqns. 27-28 models capacity limits on the production of NH3 from the H-B synthesis loop in the general case when the H-B synthesis loop is assumed to have some flexibility. The variable $\Omega_{h,t}^{HB+}$ in the right hand of Eqn. 27-28 is a continuous variable, representing the product of the binary variable v_t^{HB} and the continuous variable, Ω_h^{HB}. This product cannot be defined explicitly, since it will lead to a bilinear expression involving two variables. Instead, we enforce this definition via the Glover's Linearization as per the set of constraints in Eqn. 29 (also referred McCormick Envelopes constraints for bilinear expressions, which is exact when one of the variables is binary).

$$\Lambda_{h,t}^{HB} \leq \Omega_{h,t}^{HB+} \quad \forall h \in \mathcal{HB}, \forall t \in \mathcal{T} \tag{27}$$

$$\Lambda_{h,t}^{HB} \geq \rho^{min,HB} \times \Omega_{h,t}^{HB+} \quad \forall h \in \mathcal{HB}, \forall t \in \mathcal{T} \tag{28}$$

$$\begin{aligned}
&\Omega_{h,t}^{HB+} \leq \overline{\Omega}_h^{HB} \times v_t^{HB} \quad \forall h \in \mathcal{HB}, \forall t \in \mathcal{T} \\
&\Omega_{h,t}^{HB+} \geq \underline{\Omega}_h^{HB} \times v_t^{HB} \quad \forall h \in \mathcal{HB}, \forall t \in \mathcal{T} \\
&\Omega_{h,t}^{HB+} \geq \Omega_h^{HB} - \left(1 - v_t^{HB}\right) \times \overline{\Omega}_h^{HB} \quad \forall h \in \mathcal{HB}, \forall t \in \mathcal{T} \\
&\Omega_{h,t}^{HB+} \leq \Omega_h^{HB} - \left(1 - v_t^{HB}\right) \times \underline{\Omega}_h^{HB} \quad \forall h \in \mathcal{HB}, \forall t \in \mathcal{T}
\end{aligned} \tag{29}$$

If the H-B synthesis loop is inflexible, the variable $v_t^{HB} = 1$ for all time periods when the plant is online and the rest of the constraints are simplified accordingly.

Eqns. 30 keeps track of when HB synthesis loop is online and online, with constraint for the first period of the year looking back at the plant status in the last period (year length given by τ^{ops}) of the year. Eqns. 31 enforces that when plant is shut down, it should remain shut down for at least τ^{plant} number of hours. Eqn. 32 ensures that when the plant is offline, the H-B synthesis loop is also offline. Eqns. 33 - 33 constrain the rate of change in production output from one hour to the next. For these constraints, the implementation for $t = 1$ is based on looking at back at the production rate in the last time step of the year

similar to the formulation of minimum downtime constraint shown in Eqn. 31.

$$v_{h,t}^{HB} = v_{h,t-1}^{HB} + \chi_{h,t}^{HB} - \zeta_{h,t}^{HB} \quad \forall h \in \mathcal{HB}, t \in \{\mathcal{T}|t \neq 1\}$$

$$v_{h,t}^{HB} = v_{h,t+\tau^{ops}-1}^{HB} + \chi_{h,t}^{HB} - \zeta_{h,t}^{HB} \quad \forall h \in \mathcal{HB}, t \in \{\mathcal{T}|t = 1\} \tag{30}$$

$$1 - v_{h,t}^{HB} \geq \sum_{r \in [t-\tau_h^{HB}, t]} \zeta_{h,r}^{HB} \quad \forall h \in \mathcal{HB}, t \in \{\mathcal{T}|t > \tau_{plant}\}$$

$$1 - v_{h,t}^{HB} \geq \sum_{r \in [1,t]} \zeta_{h,r}^{HB} + \sum_{r \in [\tau^{ops} - \tau_h^{HB} - t, \tau^{ops}]} \zeta_{r,h}^{HB} \quad \forall h \in \mathcal{H}, t \in \{\mathcal{T}|t \leq \tau_{plant}\} \tag{31}$$

$$v_{h,t}^{HB} \leq v_t^{Plant} \quad \forall h \in \mathcal{H}, t \in \mathcal{T} \tag{32}$$

$$\Lambda_{h,t}^{HB} - \Lambda_{h,t-1}^{HB} \leq \kappa_h^{HB} \times \Omega_h^{HB} \quad \forall h \in \mathcal{H}, t \in \{\mathcal{T}|t > 1\} \tag{33}$$

$$\Lambda_{h,t-1}^{HB} - \Lambda_{h,t}^{HB} \leq \kappa_h^{HB} \times \Omega_h^{HB} \quad \forall h \in \mathcal{H}, t \in \{\mathcal{T}|t > 1\} \tag{34}$$

NH3 liquefaction

The NH3 liquefaction unit is modeled as a single flash unit that uses as a refrigeration system to condense out the product NH3. The liquefaction system is sized to be handle the maximum outflow from the H-B unit as per Eqn. 35. The system CAPEX is rated in terms of $ per unit of heat to be removed from the system per unit time (MW). The power requirement for the system is considered as a function of the heat duty and the coefficient of performance for the refrigeration system, as defined via Eqn. 36.

$$\sum_{h \in \mathcal{H}} \Lambda_{h,t}^{HB} \times \alpha^{\Delta H_{LIQ}} \leq \Omega_y^{LIQ} \quad \forall y \in \mathcal{LIQ}, t \in \mathcal{T} \tag{35}$$

$$\sum_{h \in \mathcal{H}} \Lambda_{h,t}^{HB} \times \beta_y^{LIQ} = \Pi_{y,t}^{LIQ} \quad \forall y \in \mathcal{LIQ}, t \in \mathcal{T} \tag{36}$$

SI 4. Thermochemical Ammonia Synthesis Loop Process Model

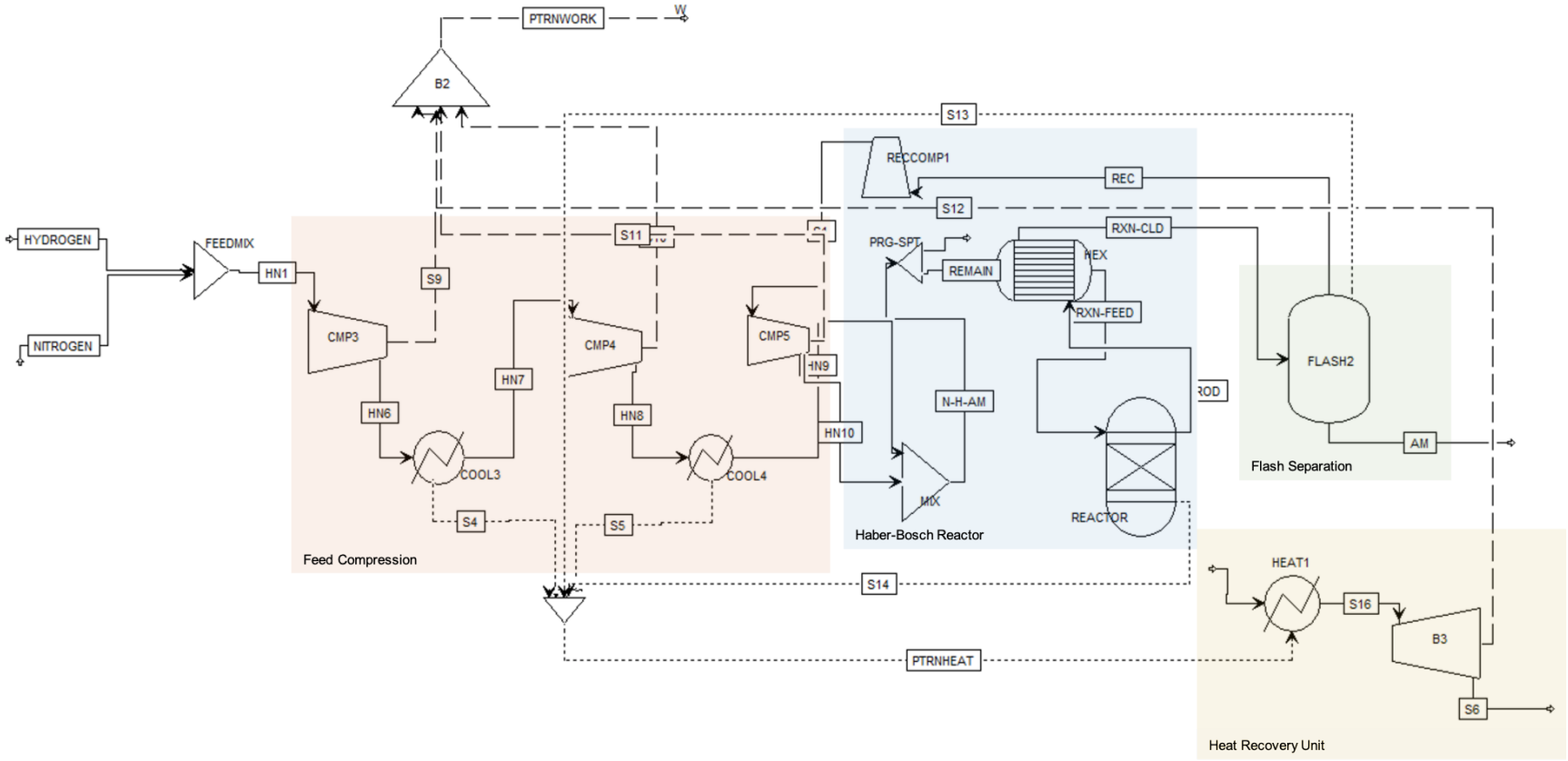

Figure SI 10: ASPEN Flowsheet for H-B Synthesis Loop Process Model

Table SI 8: Process Heater Summary

Heater			
Name	**COOL3**	**COOL4**	**HEAT1**
Property method	**RKS-BM**	**RKS-BM**	**RKS-BM**
Use true species approach for electrolytes	**YES**	**YES**	**YES**
Free-water phase properties method	**STEAM-TA**	**STEAM-TA**	**STEAM-TA**
Water solubility method	**3**	**3**	**3**
Specified pressure [bar]	**0**	**0**	**100**
Specified temperature [C]	**50**	**50**	
EO Model components			
Calculated pressure [bar]	30	81	6.89
Calculated temperature [C]	50	50	164.83
Calculated vapor fraction	1	1	0.28
Calculated heat duty [J/sec]	698668	-3393340	36268220
Pressure-drop correlation parameter			
Net duty [J/sec]	698668	-3393340	0

Table SI 9: Heat Exchanger

HeatX	
Name	**HEX**
Hot side property method	**RKS-BM**
Hot side Henry's component list ID	
Hot side electrolyte chemistry ID	
Hot side use true species approach for electrolytes	**YES**
Hot side free-water phase properties method	**STEAM-TA**
Hot side water solubility method	**3**
Cold side property method	**RKS-BM**
Cold side Henry's component list ID	
Cold side electrolyte chemistry ID	
Cold side use true species approach for electrolytes	**YES**
Cold side free-water phase properties method	**STEAM-TA**
Cold side water solubility method	**3**
Exchanger specification	**330**
Units of exchanger specification	**C**
Inlet hot stream temperature [C]	500
Inlet hot stream pressure [bar]	250
Inlet hot stream vapor fraction	1
Outlet hot stream temperature [C]	247.45
Outlet hot stream pressure [bar]	250
Outlet hot stream vapor fraction	1
Inlet cold stream temperature [C]	89.93
Inlet cold stream pressure [bar]	250
Inlet cold stream vapor fraction	1
Outlet cold stream temperature [C]	330
Outlet cold stream pressure [bar]	250
Outlet cold stream vapor fraction	1
Heat duty [J/sec]	17302759
Calculated heat duty [J/sec]	17302759
Required exchanger area [sqm]	124.38
Actual exchanger area [sqm]	124.38
Average U (Dirty) [J/sec-sqcm-K]	0.08
Average U (Clean)	
UA [J/sec-K]	105710.58
LMTD (Corrected) [C]	163.68
LMTD correction factor	1
Number of shells in series	1
Number of shells in parallel	

Table SI 10: Flash Unit

Flash2	
Name	**FLASH2**
Property method	**RKS-BM**
Use true species approach for electrolytes	**YES**
Free-water phase properties method	**STEAM-TA**
Water solubility method	**3**
Temperature [C]	**-14.3**
Pressure [bar]	**170**
Specified vapor fraction	
Specified heat duty [J/sec]	**0**
EO Model components	
Outlet temperature [C]	-14.3
Outlet pressure [bar]	170
Vapor fraction	0.80
Heat duty [J/sec]	-25049343
Net duty [J/sec]	-25049343
First liquid / total liquid	1

Table SI 11: Compressor

	Compr				
Name	**B3**	**CMP3**	**CMP4**	**CMP5**	**RECCOMP1**
Property method	**RKS-BM**	**RKS-BM**	**RKS-BM**	**RKS-BM**	**RKS-BM**
Henry's component list ID					
Electrolyte chemistry ID					
Use true species approach for electrolytes	**YES**	**YES**	**YES**	**YES**	**YES**
Free-water phase properties method	**STEAM-TA**	**STEAM-TA**	**STEAM-TA**	**STEAM-TA**	**STEAM-TA**
Water solubility method	**3**	**3**	**3**	**3**	**3**
Model Type	**ASME-ISENTROP**	**ISENTROPIC**	**ASME-ISENTROP**	**ASME-ISENTROP**	**ASME-ISENTROP**
Specified discharge pressure [bar]	**1**	**30**	**81**	**250**	**250**
Isentropic efficiency	**0.7**				
Indicated horsepower [kW]	-2207.68	0	3413.33	4168.89	2221.25
Calculated brake horsepower [kW]	-2207.68	0	3413.33	4168.89	2221.25
Net work required [kW]	-2207.68	0	3413.33	4168.89	2221.25
Efficiency (polytropic / isentropic) used	0.7	0.72	0.72	0.72	0.72
Calculated discharge pressure [bar]	1	30	81	250	250
Calculated pressure change [bar]	5.89475729	0	51	169	80
Calculated pressure ratio	0.14	1	2.7	3.08	1.47
Outlet temperature [C]	102.08	19.14	197.67	222.40	28.48
Isentropic outlet temperature [C]	102.08	19.14	156.01	172.35	16.33
Vapor fraction	0.35	1	1	1	1
Head developed [m-kgf/kg]	-11577.66	0	37667.25	46005.07	10454.92
Isentropic power requirement [kW]	-3153.83	0	2457.60	3001.60	1599.30
Inlet heat capacity ratio	1.62	1	1.41	1.42	1.49
Inlet volumetric flow rate [l/min]	136533.64	38281.47	42312.78	16155.28	13489.84
Outlet volumetric flow rate [l/min]	1029185.12	38281.47	23320.01	8555.54	11220.87
Inlet compressibility factor	0.27		1.01	1.04	1.10
Outlet compressibility factor	0.35		1.039	1.11	1.15

Table SI 12: Reactor

RGibbs	
Name	**REACTOR**
Property method	**RKS-BM**
Henry's component list ID	
Electrolyte chemistry ID	
Use true species approach for electrolytes	**YES**
Free-water phase properties method	**STEAM-TA**
Water solubility method	**3**
Specified pressure [bar]	**250**
Specified temperature [C]	**500**
Specified heat duty [J/sec]	**0**
EO Model components	
Outlet temperature [C]	500
Outlet pressure [bar]	250
Calculated heat duty [J/sec]	-8524204
Net heat duty [J/sec]	-8524204
Vapor fraction	1
Number of fluid phases	1

Table SI 13: Stream Table - Part 1 of 2

Stream Name	**Units**	**AM**	**HN1**	**HN6**	**HN7**	**HN8**	**HN9**	**HN10**	**HYDROGEN**	**N-H-AM**	**NITROGEN**
Description											
From		MAINSEP	FEEDMIX	CMP3	COOL3	CMP4	COOL4	CMP5		MIX	
To			CMP3	COOL3	CMP4	COOL4	CMP5	MIX	FEEDMIX	PRG-SPT	FEEDMIX
Stream Class		CONVEN	CONVEN	CONVEN	CONVEN	CONVEN	CONVEN	CONVEN	CONVEN	CONVEN	CONVEN
Maximum Relative Error											
Cost Flow	$/hr										
MIXED Substream											
Phase		Liquid Phase	Vapor Phase	Vapor Phase	Vapor Phase	Vapor Phase	Vapor Phase	Vapor Phase	Vapor Phase	Vapor Phase	Vapor Phase
Temperature	C	-14.30	19.14	19.14	50.00	197.67	50.00	222.41	20.00	89.93	20.00
Pressure	bar	170.00	30.00	30.00	30.00	81.00	81.00	250.00	30.00	250.00	30.00
Molar Vapor Fraction		0.00	1.00	1.00	1.00	1.00	1.00	1.00	1.00	1.00	1.00
Molar Liquid Fraction		1.00	0.00	0.00	0.00	0.00	0.00	0.00	0.00	0.00	0.00
Molar Solid Fraction		0.00	0.00	0.00	0.00	0.00	0.00	0.00	0.00	0.00	0.00
Mass Vapor Fraction		0.00	1.00	1.00	1.00	1.00	1.00	1.00	1.00	1.00	1.00
Mass Liquid Fraction		1.00	0.00	0.00	0.00	0.00	0.00	0.00	0.00	0.00	0.00
Mass Solid Fraction		0.00	0.00	0.00	0.00	0.00	0.00	0.00	0.00	0.00	0.00
Molar Enthalpy	J/mol	-291,132	-715	-715	3,065	21,528	3,170	25,720	-497	5,278	-1,363
Mass Enthalpy	J/gm	-17,034	-83	-83	356	2,504	369	2,991	-246	565	-48
Molar Entropy	J/mol-K	-836	-101	-101	-89	-77	-124	-110	-120	-153	-121
Mass Entropy	J/gm-K	-48.94	-11.72	-11.72	-10.29	-8.96	-14.40	-12.84	-59.64	-16.35	-4.29
Molar Density	mol/cc	0.03	0.00	0.00	0.00	0.00	0.00	0.01	0.00	0.01	0.00
Mass Density	gm/cc	0.53	0.01	0.01	0.01	0.02	0.02	0.05	0.00	0.07	0.03
Enthalpy Flow	J/sec	-26,613,989	-132,142	-132,142	566,526	3,979,213	585,873	4,753,974	-68,641	3,004,348	-63,501
Average MW		17.09	8.60	8.60	8.60	8.60	8.60	8.60	2.02	9.34	28.13
Mole Flows	kmol/hr	1,377.59	2,785.42	2,785.42	2,785.42	2,785.42	2,785.42	2,785.42	2,083.33	8,577.97	702.08
H2	kmol/hr	5.55	2,083.33	2,083.33	2,083.33	2,083.33	2,083.33	2,083.33	2,083.33	6,162.93	0.00
N2	kmol/hr	1.99	695.06	695.06	695.06	695.06	695.06	695.06	0.00	2,119.99	695.06
NH3	kmol/hr	1,363.75	0.00	0.00	0.00	0.00	0.00	0.00	0.00	152.53	0.00
AR	kmol/hr	6.31	7.02	7.02	7.02	7.02	7.02	7.02	0.00	142.51	7.02
CW	kmol/hr	0.00	0.00	0.00	0.00	0.00	0.00	0.00	0.00	0.00	0.00
Mole Fractions											
H2		0.00	0.75	0.75	0.75	0.75	0.75	0.75	1.00	0.72	0.00
N2		0.00	0.25	0.25	0.25	0.25	0.25	0.25	0.00	0.25	0.99
NH3		0.99	0.00	0.00	0.00	0.00	0.00	0.00	0.00	0.02	0.00
AR		0.00	0.00	0.00	0.00	0.00	0.00	0.00	0.00	0.02	0.01
CW		0.00	0.00	0.00	0.00	0.00	0.00	0.00	0.00	0.00	0.00

Table SI 14: Stream Table - Part 2 of 2

		Material									
Stream Name	**Units**	**PURGE**	**REC**	**REMAIN**	**RXN-CLD**	**RXN-FEED**	**RXN-PROD**	**S1**	**S6**	**S15**	**S16**
Description											
From		PRG-SPT	MAINSEP	PRG-SPT	HEX	HEX	REACTOR	RECCOMP1	B3		HEAT1
To			RECCOMP	HEX	MAINSEP	REACTOR	HEX	MIX		HEAT1	B3
Stream Class		CONVEN	CONVEN	CONVEN	CONVEN	CONVEN	CONVEN	CONVEN	CONVEN	CONVEN	CONVEN
Maximum Relative Error											
Cost Flow	$/hr										
MIXED Substream											
Phase		Vapor Phase	Vapor Phase	Vapor Phase	Vapor Phase	Vapor Phase	Vapor Phase	Vapor Phase		Liquid Phase	
Temperature	C	89.93	-14.30	89.93	247.45	330.00	500.00	28.49	102.08	25.00	164.83
Pressure	bar	250.00	170.00	250.00	250.00	250.00	250.00	250.00	1.00	1.00	6.89
Molar Vapor Fraction		1.00	1.00	1.00	1.00	1.00	1.00	1.00	0.36	0.00	0.29
Molar Liquid Fraction		0.00	0.00	0.00	0.00	0.00	0.00	0.00	0.64	1.00	0.71
Molar Solid Fraction		0.00	0.00	0.00	0.00	0.00	0.00	0.00	0.00	0.00	0.00
Mass Vapor Fraction		1.00	1.00	1.00	1.00	1.00	1.00	1.00	0.36	0.00	0.29
Mass Liquid Fraction		0.00	0.00	0.00	0.00	0.00	0.00	0.00	0.64	1.00	0.71
Mass Solid Fraction		0.00	0.00	0.00	0.00	0.00	0.00	0.00	0.00	0.00	0.00
Molar Enthalpy	J/mol	1,261	-2,468	1,261	-2,779	8,559	5,908	-1,087	-266,716	-288,806	-265,285
Mass Enthalpy	J/gm	135	-255	135	-250	917	532	-112	-14,805	-16,031	-14,726
Molar Entropy	J/mol-K	-36	-44	-36	-41	-21	-28	-43	-110	-171	-112
Mass Entropy	J/gm-K	-3.91	-4.54	-3.91	-3.73	-2.25	-2.51	-4.41	-6.10	-9.49	-6.19
Molar Density	mol/cc	0.01	0.01	0.01	0.01	0.00	0.00	0.01	0.00	0.04	0.00
Mass Density	gm/cc	0.07	0.07	0.07	0.06	0.04	0.04	0.08	0.00	0.76	0.01
Enthalpy Flow	J/sec	15,022	-3,970,551	2,989,327	-5,535,196	20,292,086	11,767,563	-1,749,626	-411,249,925	-445,310,881	-409,042,661
Average MW		9.34	9.69	9.34	11.12	9.34	11.12	9.69	18.02	18.02	18.02
Mole Flows	kmol/hr	42.89	5,792.74	8,535.08	7,170.33	8,535.08	7,170.33	5,792.55	5,550.84	5,550.84	5,550.84
H2	kmol/hr	30.81	4,079.64	6,132.12	4,085.19	6,132.12	4,085.19	4,079.60	0.00	0.00	0.00
N2	kmol/hr	10.60	1,425.07	2,109.39	1,427.07	2,109.39	1,427.07	1,424.93	0.00	0.00	0.00
NH3	kmol/hr	0.76	152.54	151.77	1,516.29	151.77	1,516.29	152.53	0.00	0.00	0.00
AR	kmol/hr	0.71	135.48	141.79	141.79	141.79	141.79	135.49	0.00	0.00	0.00
CW	kmol/hr	0.00	0.00	0.00	0.00	0.00	0.00	0.00	5,550.84	5,550.84	5,550.84
Mole Fractions											
H2		0.72	0.70	0.72	0.57	0.72	0.57	0.70	0.00	0.00	0.00
N2		0.25	0.25	0.25	0.20	0.25	0.20	0.25	0.00	0.00	0.00
NH3		0.02	0.03	0.02	0.21	0.02	0.21	0.03	0.00	0.00	0.00
AR		0.02	0.02	0.02	0.02	0.02	0.02	0.02	0.00	0.00	0.00
CW		0.00	0.00	0.00	0.00	0.00	0.00	0.00	1.00	1.00	1.00

References

(1) Belzer, D. B.; Cort, K. A.; Ganguli, S. A Comprehensive System of Energy Intensity Indicators for the U.S.: Methods, Data and Key Trends.

(2) Bartels, J. R. A feasibility study of implementing an Ammonia Economy. Ph.D. thesis, Iowa State University, 2008.

(3) Chehade, G.; Dincer, I. Progress in green ammonia production as potential carbon-free fuel. *Fuel 299*, 120845.

(4) Xue, M.; Wang, Q.; Lin, B.-L.; Tsunemi, K. Assessment of Ammonia as an Energy Carrier from the Perspective of Carbon and Nitrogen Footprints. *ACS Sustainable Chemistry & Engineering 7*, 12494–12500, Publisher: American Chemical Society.

(5) IEA, The Future of Hydrogen. *IEA* **2019**,

(6) Fertilizer Price Increases for 2021 Production. `https://farmdocdaily.illinois.edu/2021/04/fertilizer-price-increases-for-2021-production.html`, Accessed: 2021-04-20.

(7) Fertiliser shortage looms as global prices skyrocket. `https://indianexpress.com/article/business/fertiliser-shortage-looms-as-global-prices-skyrocket-7440556/`, Accessed: 2021-09-18.

(8) Ammonia and urea cash cost, Yara International. `https://www.yara.com/investor-relations/analyst-information/calculators/ammonia-and-urea-cash-cost/`, Accessed: 2021-08-03.

(9) Fertilizer Use in Africa: A Price Issue. `https://www.policycenter.ma/publications/fertilizer-use-africa-price-issue`, Accessed: 2021-08-03.

(10) Yara plans green ammonia production in Norway. https://www.argusmedia.com/en/news/2166590-yara-plans-green-ammonia-production-in-norway, Accessed: 2021-07-12.

(11) CF plans green ammonia plant in Louisiana. https://cen.acs.org/energy/hydrogen-power/CF-plans-green-ammonia-plant/98/i43, Accessed: 2021-07-12.

(12) Green ammonia in Australia, Spain, and the United States. https://www.ammoniaenergy.org/articles/green-ammonia-in-australia-spain-and-the-united-states/, Accessed: 2021-07-12.

(13) Saudi Arabia to export renewable energy using green ammonia. https://www.ammoniaenergy.org/articles/saudi-arabia-to-export-renewable-energy-using-green-ammonia/, Accessed: 2021-07-12.

(14) MacFarlane, D. R.; Cherepanov, P. V.; Choi, J.; Suryanto, B. H. R.; Hodgetts, R. Y.; Bakker, J. M.; Vallana, F. M. F.; Simonov, A. N. A Roadmap to the Ammonia Economy. *Joule* **2020**, *4*, 1186–1205, Publisher: Elsevier.

(15) Wang, M.; Khan, M. A.; Mohsin, I.; Wicks, J.; Ip, A. H.; Sumon, K. Z.; Dinh, C.-T.; Sargent, E. H.; Gates, I. D.; Kibria, M. G. Can sustainable ammonia synthesis pathways compete with fossil-fuel based Haber–Bosch processes? *Energy & Environmental Science* **2021**, *14*, 2535–2548, Publisher: The Royal Society of Chemistry.

(16) Salmon, N.; Bañares-Alcántara, R. Green ammonia as a spatial energy vector: a review. *Sustainable Energy & Fuels* **2021**, *5*, 2814–2839, Publisher: Royal Society of Chemistry.

(17) Comer, B. M.; Fuentes, P.; Dimkpa, C. O.; Liu, Y.-H.; Fernandez, C. A.; Arora, P.; Realff, M.; Singh, U.; Hatzell, M. C.; Medford, A. J. Prospects and Challenges for Solar Fertilizers. *Joule* **2019**, *3*, 1578–1605.

(18) Dias, V.; Pochet, M.; Contino, F.; Jeanmart, H. Energy and Economic Costs of Chemical Storage. *Frontiers in Mechanical Engineering* **2020**, *6*, Publisher: Frontiers.

(19) Osman, O.; Sgouridis, S.; Sleptchenko, A. Scaling the production of renewable ammonia: A techno-economic optimization applied in regions with high insolation. *Journal of Cleaner Production* **2020**, *271*, 121627.

(20) Maia, M. M. Techno-economic analysis of green ammonia production using offshore wind farms. Master of Science (M.Sc.) in Sustainable Energy Engineering, Iceland School of Energy, Reykjavík University, 2021.

(21) Nosherwani, S. A.; Neto, R. C. Techno-economic assessment of commercial ammonia synthesis methods in coastal areas of Germany. *Journal of Energy Storage* **2021**, *34*, 102201.

(22) Fúnez Guerra, C.; Reyes-Bozo, L.; Vyhmeister, E.; Jaén Caparrós, M.; Salazar, J. L.; Clemente-Jul, C. Technical-economic analysis for a green ammonia production plant in Chile and its subsequent transport to Japan. *Renewable Energy* **2020**, *157*, 404–414.

(23) Li, J.; Lin, J.; Heuser, P. M.; Heinrichs, H. U.; Xiao, J.; Liu, F.; Robinius, M.; Song, Y.; Stolten, D. Co-Planning of Regional Wind Resources-based Ammonia Industry and the Electric Network: A Case Study of Inner Mongolia. *IEEE Transactions on Power Systems* **2022**, *37*, 65–80.

(24) Pawar, N. D.; Heinrichs, H. U.; Winkler, C.; Heuser, P.-M.; Ryberg, S. D.; Robinius, M.; Stolten, D. Potential of green ammonia production in India. *International Journal of Hydrogen Energy* **2021**, *46*, 27247–27267.

(25) Nayak-Luke, R.; Bañares-Alcántara, R.; Wilkinson, I. "Green" Ammonia: Impact of Renewable Energy Intermittency on Plant Sizing and Levelized Cost of Ammonia. *Industrial & Engineering Chemistry Research* **2018**, *57*, 14607–14616.

(26) Gallardo, F. I.; Monforti Ferrario, A.; Lamagna, M.; Bocci, E.; Astiaso Garcia, D.; Baeza-Jeria, T. E. A Techno-Economic Analysis of solar hydrogen production by electrolysis in the north of Chile and the case of exportation from Atacama Desert to Japan. *International Journal of Hydrogen Energy* **2021**, *46*, 13709–13728.

(27) Liang, C. Green Haber-Bosch Process:A Small-Scale Ammonia Reactor System Design. M.Sc. thesis, Mechanical Engineering, Delft University of Technology, 2019.

(28) Osman, O.; Sgouridis, S.; Sleptchenko, A. Scaling the production of renewable ammonia: A techno-economic optimization applied in regions with high insolation. *Journal of Cleaner Production* **2020**, *271*, 121627.

(29) Michael Nayak-Luke, R.; Bañares-Alcántara, R. Techno-economic viability of islanded green ammonia as a carbon-free energy vector and as a substitute for conventional production. *Energy & Environmental Science* **2020**, *13*, 2957–2966.

(30) Morgan, E. R.; Manwell, J. F.; McGowan, J. G. Sustainable Ammonia Production from U.S. Offshore Wind Farms: A Techno-Economic Review. *ACS Sustainable Chemistry & Engineering* **2017**, *5*, 9554–9567.

(31) Zhang, H.; Desideri, U. Techno-Economic Evaluation of Power-to-Ammonia System. *Proceedings of 11th International Conference on Applied Energy* **2019**, *4*.

(32) Palys, M. J.; Daoutidis, P. Using hydrogen and ammonia for renewable energy storage: A geographically comprehensive techno-economic study. *Computers & Chemical Engineering* **2020**, *136*, 106785.

(33) Bañares-Alcántara, R.; Iii, G. D.; Fiaschetti, M.; Grünewald, P.; Lopez, J. M.; Tsang, E.; Yang, A.; Ye, L.; Zhao, S. *Analysis of Islanded Ammonia-based Energy Storage Systems*; 2015; University of Oxford.

(34) Armijo, J.; Philibert, C. Flexible production of green hydrogen and ammonia from variable solar and wind energy: Case study of Chile and Argentina. *International Journal of Hydrogen Energy* **2020**, *45*, 1541–1558.

(35) Schulte Beerbühl, S.; Fröhling, M.; Schultmann, F. Combined scheduling and capacity planning of electricity-based ammonia production to integrate renewable energies. *European Journal of Operational Research* **2015**, *241*, 851–862.

(36) Allman, A.; Daoutidis, P. Optimal scheduling for wind-powered ammonia generation: Effects of key design parameters. *Chemical Engineering Research and Design* **2018**, *131*, 5–15.

(37) Zhang, H.; Wang, L.; Van herle, J.; Maréchal, F.; Desideri, U. Techno-economic comparison of green ammonia production processes. *Applied Energy* **2020**, *259*.

(38) Mallapragada, D. S.; Gençer, E.; Insinger, P.; Keith, D. W.; O'Sullivan, F. M. Can Industrial-Scale Solar Hydrogen Supplied from Commodity Technologies Be Cost Competitive by 2030? *Cell Reports Physical Science* **2020**, 100174.

(39) Gurobi Optimization, LLC, Gurobi Optimizer Reference Manual. 2021; `https://www.gurobi.com`.

(40) Reuther, A. et al. Interactive supercomputing on 40,000 cores for machine learning and data analysis. 2018 IEEE High Performance extreme Computing Conference (HPEC). 2018; pp 1–6.

(41) IEA, GLobal Hydrogen Review 2021. *IEA* **2021**,

(42) Green hydrogen cost reduction: Scaling up electrolysers to meet the 1.5C climate goal. *International Renewable Energy Agency*

(43) Council, H. Hydrogen Insights 2021. *Hydrogen Council* **2021**,

(44) Linde, Nitrogen Generation by Pressure Swing Adsorption. 2021; https://www.leamericas.com/en/technologies/air-separation/index.html.

(45) Saavedra Lopez, J.; Lebarbier Dagle, V.; Deshmane, C. A.; Kovarik, L.; Wegeng, R. S.; Dagle, R. A. Methane and Ethane Steam Reforming over MgAl2O4-Supported Rh and Ir Catalysts: Catalytic Implications for Natural Gas Reforming Application. *Catalysts* **2019**, *9*, 801, Number: 10 Publisher: Multidisciplinary Digital Publishing Institute.

(46) Brown, P. R.; Botterud, A. The Value of Inter-Regional Coordination and Transmission in Decarbonizing the US Electricity System. *Joule* **2021**, *5*, 115–134.

(47) Akar, S.; Beiter, P.; Cole, W.; Feldman, D.; Kurup, P.; Lantz, E.; Margolis, R.; Oladosu, D.; Stehly, T.; Rhodes, G.; Turchi, C.; Vimmerstedt, L. *2020 Annual Technology Baseline (ATB) Cost and Performance Data for Electricity Generation Technologies*.

(48) Cole, W.; Corcoran, S.; Gates, N.; Mai, T.; Das, P. *2020 Standard Scenarios Report: A U.S. Electricity Sector Outlook*; 2020; p 51.

(49) Gagnon, P.; Frazier, W.; Hale, E.; Cole, W. Cambium data for 2020 Standard Scenarios. https://cambium.nrel.gov/.

(50) Smith, C. N.; Hittinger, E. Using marginal emission factors to improve estimates of emission benefits from appliance efficiency upgrades. *Energy Efficiency* **2019**, *12*, 585–600.

(51) US EPA, O. GHGRP Non-Fluorinated Chemicals. https://www.epa.gov/ghgreporting/ghgrp-non-fluorinated-chemicals.

(52) Price Gouging or Price Reality? Anhydrous Ammonia Prices Climb 60% Since Fall. https://www.agweb.com/news/crops/corn/price-gouging-or-price-reality-anhydrous-ammonia-prices-climb-60-fall.

(53) Beswick, R. R.; Oliveira, A. M.; Yan, Y. Does the green hydrogen economy have a water problem? *ACS Energy Letters* **2021**, *6*, 3167–3169.

(54) Seel, J.; Mills, A. D.; Wiser, R. H.; Deb, S.; Asokkumar, A.; Hassanzadeh, M.; Aarabali, A. Impacts of High Variable Renewable Energy Futures on Wholesale Electricity Prices, and on Electric-Sector Decision Making. `http://www.osti.gov/servlets/purl/1437006/`.

(55) Palys, M. J.; Wang, H.; Zhang, Q.; Daoutidis, P. Renewable ammonia for sustainable energy and agriculture: vision and systems engineering opportunities. *Current Opinion in Chemical Engineering* **2021**, *31*, 100667.

(56) Sengupta, M.; Xie, Y.; Lopez, A.; Habte, A.; Maclaurin, G.; Shelby, J. The National Solar Radiation Data Base (NSRDB). *Renewable and Sustainable Energy Reviews* **2018**, *89*, 51–60.

(57) F. Holmgren, W.; W. Hansen, C.; A. Mikofski, M. pvlib python: a python package for modeling solar energy systems. *Journal of Open Source Software* **2018**, *3*, 884.

(58) Dobos, A. PVWatts Version 5 Manual. `http://www.osti.gov/servlets/purl/1158421/`.

(59) Draxl, C.; Hodge, B. M.; Clifton, A.; McCaa, J. Overview and Meteorological Validation of the Wind Integration National Dataset toolkit. *National Renewable Energy Laboratory* Accessed: 2021-08-03.

(60) Draxl, C.; Clifton, A.; Hodge, B.-M.; McCaa, J. The Wind Integration National Dataset (WIND) Toolkit. *Applied Energy* **2015**, *151*, 355–366.

(61) Lieberman-Cribbin, W.; University, C. A Guide to Using the WIND Toolkit Validation Code. *National Renewable Energy Laboratory* **2014**,

(62) King, J.; Clifton, A.; Hodge, B. Validation of Power Output for the WIND Toolkit. *National Renewable Energy Laboratory* **2014**,

(63) Hydrogen from renewable power: Technology outlook for the energy transition. *International Renewable Energy Agency* **2018**,

(64) Hydrogen Delivery Infrastructure Options Analysis. `https://hdsam.es.anl.gov/index.php`, Accessed: 2019-09-16.

(65) Eichman, J.; Flores-Espino, F. California Power-to-Gas and Power-to-Hydrogen Near-Term Business Case Evaluation. *National Renewable Energy Laboratory* **2016**,

(66) Demirhan, C. D.; Tso, W. W.; Powell, J. B.; Pistikopoulos, E. N. A multi-scale energy systems engineering approach towards integrated multi-product network optimization. *Applied Energy 281*, 116020.

(67) Ahluwalia, R.; Papadias, D.; Peng, J.; Roh, H. System Level Analysis of Hydrogen Storage Options. *Argonne National Laboratory* **2020**,

(68) Kim, J.; Noh, Y.; Chang, D. Storage system for distributed-energy generation using liquid air combined with liquefied natural gas. *Applied Energy 212*, 1417–1432.

(69) *Ammonia*; John Wiley & Sons, Ltd, pp 213–220, Section: 9 _eprint: https://onlinelibrary.wiley.com/doi/pdf/10.1002/9783527613885.ch09.